Chemical Geology

The role of anaerobic oxidation of methane on the authigenic carbonate formation in sediments of the subtropical Beibu Gulf, South China Sea: A Reactive–transport modeling approach

--Manuscript Draft--

Manuscript Number:	CHEMGE15213
Article Type:	Research paper
Keywords:	Authigenic carbonate; Anaerobic oxidation of methane; Carbon isotopes; Reactive-transport modeling; Non-steady-state diagenesis
Abstract:	The formation and burial of authigenic carbonate in marine sediment is a crucial global carbon sink and significantly affects the carbon isotopic composition of sedimentary rocks in geological time. Anaerobic oxidation of methane (AOM) is the primary driver of authigenic carbonate formation within the sulfate methane transition zone (SMTZ). Quantitative estimations of the role of AOM on the authigenic carbonate formation and its carbon isotope (δ 13 C-CaCO 3) under a non-steady-state, however, are still limited. In this study, we use geochemical data from porewater (e.g., the concentration of sulfate, calcium, magnesium, strontium, dissolved inorganic carbon, total alkalinity) and solid sediment (e.g., organic matter content, carbonate content, and δ 13 C-CaCO 3) in different depositional environments of the subtropical Beibu Gulf, South China Sea, combined with a diagenetic reactive-transport modeling approach, to determine the types of authigenic carbonate, the relationship between AOM rate and authigenic carbonate formation rate, and the impact of AOM rate on δ 13 C-CaCO 3 buried in sediments. The results show that high-Mg calcite is the main type of authigenic carbonate (~80%) precipitated in the methane-bearing sediments, leading to high porewater Sr 2+ /Ca 2+ (>0.02) and Mg 2+ /Ca 2+ (>20) within the SMTZ. Our modeling analysis highlights that the non-steady-state induced by an increase of methane flux from the underlying sediments can significantly accelerate the formation of authigenic carbonates at the sulfate-methane transition zone (SMTZ). Using parametric sensitivity analysis, we observed that when the authigenic carbonate formation rate in sediments is increased by 14%, the fraction of authigenic carbonate in the total carbonates increases by 1%, and δ 13 C-CaCO 3 within the SMTZ is shifted from -1‰ to -2‰. Noteworthily, the terrestrial-to-marine transition zone was identified by the sediment geochemical profile of the site SO-8, where porewater freshening substantially impacts the authigenic carbonate formation rate. Combining global methane flux into the SMTZ, we estimate the budget of methane-derived authigenic carbonates in global marine sediments to be ~0.49 Tmol yr -1 , with about 67% occurring in continental shelf sediments (<200m water depth).

Summary of Comments on CHEMGE15213_reviewer.pdf

This page contains no comments

The role of anaerobic oxidation of methane on the authigenic carbonate formation in sediments of the subtropical Beibu Gulf, South China Sea: A Reactive–transport modeling approach

Sinan Xu[1,2], Bo Liu[2], Zijun Wu[1*], Nicole Kowalski[3], Michael E. Böttcher[3,4,5]

[1]*State Key Laboratory of Marine Geology, School of Ocean and Earth Science, Tongji University, Shanghai, 200092, P.R. China*

[2]*Alfred Wegener Institute Helmholtz Centre for Polar and Marine Research, 27570 Bremerhaven, Germany*

[3]*Geochemistry & Isotope Biogeochemistry Group, Department of Marine Geology, Leibniz Institute for Baltic Sea Research (IOW), D-18119 Warnemünde, Germany*

[4]*Marine Geochemistry, University of Greifswald, Greifswald, Germany*

[5]*Interdisciplinary Faculty, University of Rostock, Rostock, Germany*

*** Corresponding author. Email:** wuzj@tongji.edu.cn

Abstract

The formation and burial of authigenic carbonate in marine sediment is a crucial global carbon sink and significantly affects the carbon isotopic composition of sedimentary rocks in geological time. Anaerobic oxidation of methane (AOM) is the primary driver of authigenic carbonate formation within the sulfate methane transition zone (SMTZ). Quantitative estimations of the role of AOM on the authigenic carbonate formation and its carbon isotope (δ^{13}C-$CaCO_3$) under a non-steady-state, however, are still limited. In this study, we use geochemical data from porewater (e.g., the concentration of sulfate, calcium, magnesium, strontium, dissolved inorganic carbon, total alkalinity) and solid sediment (e.g., organic matter content, carbonate content, and δ^{13}C-$CaCO_3$) in different depositional environments of the subtropical Beibu Gulf, South China Sea, combined with a diagenetic reactive-transport modeling approach, to determine the types of authigenic carbonate, the relationship between AOM rate and authigenic carbonate formation rate, and the impact of AOM rate on δ^{13}C-$CaCO_3$ buried in sediments. The

Page: 2

Number: 1 Subject: Sticky Note Date: 16/07/2022 15:23:08

you exagerate here.
See Akam et al., 2020
doi:10.3389/fmars.2020.00206

Number: 2 Subject: Sticky Note Date: 16/07/2022 15:24:26

what do you mean by 'type' ?
the mineralogy ?

Number: 3 Subject: Line Date: 16/07/2022 15:24:08

Number: 4 Subject: Line Date: 16/07/2022 15:24:09

results show that high-Mg calcite is the main type of authigenic carbonate (~80%) precipitated in the methane-bearing sediments, leading to high porewater Sr^{2+}/Ca^{2+} (>0.02) and Mg^{2+}/Ca^{2+} (>20) within the SMTZ. Our modeling analysis highlights that the non-steady-state induced by an increase of methane flux from the underlying sediments can significantly accelerate the formation of authigenic carbonates at the sulfate-methane transition zone (SMTZ). Using parametric sensitivity analysis, we observed that when the authigenic carbonate formation rate in sediments is increased by 14%, the fraction of authigenic carbonate in the total carbonates increases by 1%, and $\delta^{13}C$-$CaCO_3$ within the SMTZ is shifted from -1‰ to -2‰. Noteworthily, the terrestrial-to-marine transition zone was identified by the sediment geochemical profile of the site SO-8, where porewater freshening substantially impacts the authigenic carbonate formation rate. Combining global methane flux into the SMTZ, we estimate the budget of methane-derived authigenic carbonates in global marine sediments to be ~0.49 Tmol yr^{-1}, with about 67% occurring in continental shelf sediments (<200m water depth).

Keywords: Authigenic carbonate; Anaerobic oxidation of methane; Carbon isotopes; Reactive-transport modeling; Non-steady-state diagenesis.

1.Introduction

Authigenic carbonate, the third major sedimentary sink for carbon (Schrag et al., 2013), is widely distributed in marine sediments, particularly in continental shelf regions (Bradbury and Turchyn, 2019; Sun and Turchyn, 2014). Due to the average carbon isotopic value of authigenic carbonate is about −20.5 ± 3.5 ‰, which is far less than

Page: 3

Number: 1 Subject: Sticky Note Date: 16/07/2022 15:31:12

you are mixing inforamtion about rate and amount.
You rise the rate by 14%; but for which period of time ? You need to indicate the time to move from a rate to a quantitiy (you then cite a fraction, ie a quantity of 1%).

Number: 2 Subject: Line Date: 16/07/2022 15:27:40

Number: 3 Subject: Sticky Note Date: 16/07/2022 15:27:34

?
You are on the sea floor right ? What do you mean by terrestrial?

Number: 4 Subject: Line Date: 16/07/2022 15:27:37

Number: 5 Subject: Sticky Note Date: 16/07/2022 15:30:54

are you certain ?
Cite recent and renewed reference for such a statement :
Akam et al., 2020. Dissolved Inorganic Carbon Pump in
Methane-Charged Shallow Marine
Sediments: State of the Art and New
Model Perspectivesdoi: 10.3389/fmars.2020.00206

AND
Saunois, M., Stavert, A. R., Poulter, B., Bousquet, P., Canadell, J. G., Jackson, R. B., ... & Zhuang, Q. (2020). The global methane budget 2000–2017. Earth system science data, 12(3), 1561-1623.

Number: 6 Subject: Line Date: 16/07/2022 15:30:59

that of biological carbonate (0-1 ‰) (Bradbury and Turchyn, 2019; Mitnick et al., 2018), the formation and burial of authigenic carbonate obviously impact the carbon isotope composition of carbonates (δ^{13}C-$CaCO_3$) in marine sediments. Therefore, authigenic carbonate formation in marine sediments plays a vital role in the global carbon cycle and its isotope mass balance over Earth's history (Lippmann, 1973; Mitnick et al., 2018; Morse and Mackenzie, 1990; Schrag et al., 2013; Turchyn et al., 2021; Ussler III and Paull, 2008).

The chemical reaction of authigenic carbonate formation in marine sediments is mainly through the precipitation of porewater Ca^{2+} (Eq. (1)). An estimated 1×10^{12} mol yr^{-1} net calcium flux in marine sediments is used for authigenic carbonate, accounting for at least 10% of global carbonate accumulation (Sun and Turchyn, 2014).

$$Ca^{2+} + 2HCO_3^- \leftrightarrow CaCO_3 + CO_2 + H_2O \quad (1)$$

From the chemical viewpoint, the formation of authigenic carbonate is closely related to the acid-base equilibrium system of porewater (Soetaert et al., 2007; Zeebe and Wolf-Gladrow, 2001). Higher pH triggers the formation of authigenic carbonate in sediments, releasing carbon dioxide and lowering pH (Luff et al., 2001). Carbonate (CO_3^{2-}), along with bicarbonate (HCO_3^-) and carbon dioxide (CO_2), is a crucial chemical parameter in maintaining the porewater acid-base balance. Consequently, the dissolved inorganic carbon (DIC, Eq. (2)) and total alkalinity (TA, Eq. (3)) are significant for the formation of authigenic carbonate in marine sediment (Zeebe and Wolf-Gladrow, 2001). According to the porewater carbonate equilibrium system, knowing two of TA, DIC, and pH can calculate the other one (Brand and Veizer, 1980; Middelburg et al., 2020;

Page: 4

Number: 1 Subject: Sticky Note Date: 16/07/2022 15:33:30

I recomment that you cite:
Peckmann, J., & Thiel, V. (2004). Carbon cycling at ancient methane–seeps. Chemical Geology, 205(3-4), 443-467.

Number: 2 Subject: Sticky Note Date: 16/07/2022 15:36:53

I think you are exageratig. Let's keep raisonable.
otherwise, provide numbers to support your assertion.

Number: 3 Subject: Line Date: 16/07/2022 15:33:48

Number: 4 Subject: Line Date: 16/07/2022 15:33:50

Number: 5 Subject: Sticky Note Date: 16/07/2022 15:37:36

"the reaction of precipitation"

Number: 6 Subject: Line Date: 16/07/2022 15:38:30

Number: 7 Subject: Line Date: 16/07/2022 15:37:51

Number: 8 Subject: Sticky Note Date: 16/07/2022 15:39:04

??????????
CaCO3
Why Ca is more imporant than CO3.
In addition, Ca2+ is rarely a limitant factor for the precipitation oa authiigeni carbontes.

Number: 9 Subject: Line Date: 16/07/2022 15:38:28

Number: 10 Subject: Line Date: 16/07/2022 15:37:53

Number: 11 Subject: Sticky Note Date: 16/07/2022 15:42:15

Check more recent papers:

Bradbury, H. J., and Turchyn, A. V. (2019). Reevaluating the carbon sink due to sedimentary carbonate formation in modern marine sedim

Akam, S. A., Coffin, R. B., Abdulla, H. A., & Lyons, T. W. (2020). Dissolved inorganic carbon pump in methane-charged shallow marine sediments: state of the art and new model perspectives. Frontiers in Marine Science, 7, 206.

Number: 12 Subject: Sticky Note Date: 16/07/2022 15:43:32

here you must cite:
Jourabchi, Parisa, Philippe Van Cappellen, and Pierre Regnier. "Quantitative interpretation of pH distributions in aquatic sediments: A reaction-transport modeling approach." American Journal of Science 305, no. 9 (2005): 919-956.

AND

Blouet, J. P., Arndt, S., Imbert, P., & Regnier, P. (2021). Are seep carbonates quantitative proxies of CH4 leakage? Modeling the influence of sulfate reduction and anaerobic oxidation of methane on pH and carbonate precipitation. Chemical Geology, 577, 120254.

Number: 13 Subject: Pencil Date: 16/07/2022 15:45:28

Number: 14 Subject: Sticky Note Date: 16/07/2022 15:45:34

here you explaction of the carbonate system is not clear.
Have a look at :
Blouet, J. P., Arndt, S., Imbert, P., & Regnier, P. (2021). Are seep carbonates quantitative proxies of CH4 leakage? Modeling the influence of sulfate reduction and anaerobic oxidation of methane on pH and carbonate precipitation. Chemical Geology, 577, 120254.

Millero, 1979; Millero, 1995; Zeebe and Wolf-Gladrow, 2001).

$$[DIC] = [CO_2] + [HCO_3^-] + [CO_2^{2-}] \tag{2}$$

$$[TA] = [HCO_3^-] + 2 \cdot [CO_2^{2-}] + [HS^-] - [H^+] + minor \tag{3}$$

where minor included borate, phosphate, silicate, etc., and their concentration in the porewater is ~~far low~~ than the bicarbonate and carbonate (Middelburg et al., 2020), ~~and square brackets indicate concentration~~.

The major factors affecting the porewater pH, DIC, and TA are biogeochemical processes occurring in marine sediments, i.e., organoclastic sulfate reduction (OSR, Eq. (4)), methanogenesis (ME) and anaerobic oxidation of methane (AOM, Eq. (5)). These processes consume or produce carbonate, bicarbonate, and carbon dioxide, resulting in variations in porewater pH (Soetaert et al., 2007).

$$2CH_2O + SO_4^{2-} \rightarrow 2HCO_3^- + H_2S \tag{4}$$

$$CH_4 + SO_4^{2-} \rightarrow HCO_3^- + HS^- + H_2O \tag{5}$$

Several studies on authigenic carbonate formation in global marine sediments have been conducted. Sun et al. (2014) estimated the contribution of authigenic carbonate to marine carbon burial on a global scale by simulating porewater Ca^{2+} concentrations at 672 sites using linear regression and simple polyline fitting methods without considering biogeochemical reactions and porewater diffusion and advection processes. Mitnick et al. (2018) calculated the rate of authigenic carbonate formation within different depositional environments using an advection-diffusion equation based on the porewater data (e.g., concentrations of Ca^{2+}, Mg^{2+}, SO_4^{2-} and other variables) collected from 37 sites under steady-state, where biogeochemical reactions were still ignored.

Page: 5

Number: 1 Subject: Sticky Note Date: 16/07/2022 15:46:12
good to ref to Millero.

Number: 2 Subject: Sticky Note Date: 16/07/2022 15:47:05
how many orders of magnitude ?

Number: 3 Subject: Line Date: 16/07/2022 15:46:31

Number: 4 Subject: Line Date: 16/07/2022 15:46:56

Number: 5 Subject: Line Date: 16/07/2022 15:46:59

Number: 6 Subject: Sticky Note Date: 16/07/2022 15:46:55
obiously

Number: 7 Subject: Sticky Note Date: 16/07/2022 15:49:36
To justify that you discard minor diagenetic reaction, you car refere to:
Dale, A.W., Brüchert, V., Alperin, M., Regnier, P., 2009. An integrated sulfur isotope model for Namibian shelf sediments. Geochim. Cosmochim. Acta 73, 1924 – 1944.

aND

Thullner, M., Regnier, P., 2019. Microbial Controls on the Biogeochemical Dynamics in the Subsurface. Rev. Mineral. Geochem. 85, 265 – 302.

Number: 8 Subject: Sticky Note Date: 16/07/2022 15:52:49
mention that this is the simplified formula of organic matter.

Arndt, S., Jørgensen, B. B., LaRowe, D. E., Middelburg, J. J., Pancost, R. D., & Regnier, P. (2013). Quantifying the degradation of organic matter in marine sediments: A review and synthesis. Earth-science reviews, 123, 53-86.

Number: 9 Subject: Sticky Note Date: 16/07/2022 15:53:58
several "modeling" studies

Number: 10 Subject: Sticky Note Date: 16/07/2022 15:54:01
again, see the more modern reference mentionned above.

Additionally, the reactive-transport modeling (RTM) with a fitting function that minimizes the difference between the measured and simulated concentrations was used to estimate the formation rate of authigenic carbonate (Chuang et al., 2019; Wallmann et al., 2006). The numerical model CANDI (Calcite, Carbon And Nutrient Diagenesis) was also used to estimate the formation of authigenic carbonate in the Cascadia Margin and the Arabian Sea by simulating the pH distribution in the porewater (Boudreau, 1996; Luff et al., 2005; Luff and Wallmann, 2003; Luff et al., 2000). Recently, Blouet et al. (2021) estimated the formation of authigenic carbonate by an RTM that describes the contribution of biogeochemical reactions to the change in porewater pH and the saturation state of calcium carbonate minerals. Although the modeling studies mentioned above confirmed that AOM is conducive to promoting the formation of authigenic carbonate, these studies all assumed ~~that under~~ steady-state conditions and obviously cannot well reflect the actual sedimentary condition in marine sediments. For example, hydrates are typically buried in continental shelf regions at water depths greater than 200 m (Buffett and Archer, 2004; Kvenvolden, 1993). The complex depositional environment in these regions may induce hydrate destabilization (e.g., changes in temperature and pressure in the underlying sediments), resulting in an increase in methane concentration in the underlying overlying porewater (Phrampus and Hornbach, 2012; Suess et al., 199 , altering the AOM process in the sediments and further affecting the formation of authigenic carbonates in the sediments. Until now, limited attempts have been made to evaluate the authigenic carbonate formation and its impact on $\delta^{13}C$-$CaCO_3$ under a non-steady-state depositional environment

Page: 6

Number: 1 Subject: Sticky Note Date: 16/07/2022 15:56:31

You amy give some results from thoses studies: which rate of precipitation did they obtained ?

Number: 2 Subject: Sticky Note Date: 16/07/2022 15:59:49

Yes; good to cite those important references.
But, they are all dealing with seep site; ie an area of the sea floor with focussed advection of methane. This in not the 'regular' sea floor.
Do you work at seep site only, or on the entier sediment surface (seep site, and non-seep sites) ?

Number: 3 Subject: Line Date: 16/07/2022 15:56:55

Number: 4 Subject: Line Date: 16/07/2022 15:56:53

Number: 5 Subject: Sticky Note Date: 16/07/2022 15:57:36

you don't explain why the presence of hydrate whould be a problem to be described at steady state.

Number: 6 Subject: Sticky Note Date: 16/07/2022 16:01:06

ok, you aswert to my previous comment;
rephrase.

Number: 7 Subject: Sticky Note Date: 16/07/2022 16:01:08

De La Fuente, M., Arndt, S., Marín-Moreno, H., & Minshull, T. A. (2022). Assessing the Benthic Response to Climate-Driven Methane Hydrate Destabilisation: State of the Art and Future Modelling Perspectives. Energies, 15(9), 3307.

Number: 8 Subject: Sticky Note Date: 16/07/2022 16:02:29

check and cite:

Aloisi, G., Wallmann, K., Haese, R. R., & Saliege, J. F. (2004). Chemical, biological and hydrological controls on the 14C content of cold seep carbonate crusts: numerical modeling and implications for convection at cold seeps. Chemical Geology, 213(4), 359-383.

In this study, we use the measured geochemical composition of porewater (e.g., sulfate, calcium, magnesium, strontium, DIC, and TA) and solid sediments (e.g., organic carbon, carbonate content, and $\delta^{13}C$-$CaCO_3$), to simulate the rates of AOM and the authigenic carbonate formation by RTM in Beibu Gulf, South China Sea. The Beibu Gulf is a typical subtropical region characterized by a highly complex depositional system in a shallow shelf sea with active coastal mangrove systems (Li et al., 2010; Tang et al., 2008; Wu et al., 2018). Organic matter transported by inland rivers (e.g., Red River, Qingjiang River, and the Nanliu River) provides sufficient substrates for methanogenesis in deep sediments (Trung, 2012; Wang et al., 2018; Yang et al., 2015; Zhang et al., 2015). Previous geochemical and modeling studies have proved that the study area is in a non-steady-state system (Wu et al., 2018). The study aims to quantitatively evaluate the impact of AOM on authigenic carbonate and its carbon isotopic composition under a non-steady-state depositional environment of the Beibu Gulf, South China Sea, and estimate the budget of methane-derived authigenic carbonates formation in global marine sediments based on the relationship between AOM and authigenic carbonate.

2.Materials and methods

2.1 Study area

The Beibu Gulf, located in the northwest of the South China Sea, is a typical subtropical gulf (Bauer et al., 2013; Wu et al., 2018) and is a shallow shelf sea region with an average depth of around 45 meters and a maximum depth of about 100 meters (Tanabe

Page: 7

Number: 1 Subject: Rectangle Date: 16/07/2022 16:05:35

Number: 2 Subject: Rectangle Date: 16/07/2022 16:05:37

Number: 3 Subject: Arrow Date: 16/07/2022 16:05:57

Number: 4 Subject: Arrow Date: 16/07/2022 16:06:22

Number: 5 Subject: Sticky Note Date: 16/07/2022 16:10:31

keep those information for the §Study Area, and be more brief here. Or explain why subtropical region are interesting for your question.
Why select this site rather than an other one ?

Number: 6 Subject: Text Box Date: 16/07/2022 16:06:19

repetition

Number: 7 Subject: Sticky Note Date: 16/07/2022 16:08:55

OK. you also answer to one of my question above: seep vs. non-seep site !
Make clear what is a seep and a non-seep site earlyer in the introduction.
For exemple; check the introductio of the paper below and cite it:

Blouet, Jean-Philippe, Patrice Imbert, Anneleen Foubert, Sutieng Ho, and Gerard Dupont. "From seep carbonates down to petroleum systems: An outcrop study from the southeastern France Basin." AAPG bulletin 105, no. 5 (2021): 1033-1064.

Number: 8 Subject: Rectangle Date: 16/07/2022 16:05:43

Number: 9 Subject: Rectangle Date: 16/07/2022 16:05:45

Number: 10 Subject: Rectangle Date: 16/07/2022 16:05:47

et al., 2003; Wu et al., 2008). ~~The location of the study sites and their water depth is shown in~~ (Fig.1 and Table 1) According to the mineral analysis, the Red River provides most of the sediments in the western area, and the depositional process is greatly affected by coastal erosion along the shore. By contrast, vast sediments in the southern area are carried by ocean currents (Chen and Zhang, 1986). Thus, the central region of the Beibu Gulf consists of fine-grained sediments that are gradually replaced by sandy sediments closer to the coast. The grain size, contents of marine organisms, and sedimentary structures, as well as porewater and sediment geochemistry in the Beibu Gulf and its coastal area, ~~have been reported by previous literatures~~ (Bauer et al., 2013; Kaiser et al., 2015; Leipe et al., 2011; Wu et al., 2018).

2.2 Sampling and analytical methods

During the joint German-Chinese expedition SONNE219 (December 2011), five sediment cores (SO-8, SO-23, SO-26, SO-45, and SO-50) were collected using a Gravity core sampler in the study area. All sampling techniques and analytical methods, along with porewater solute concentrations (Cl^-, SO_4^{2-}, Ca^{2+}, Mg^{2+}, DIC, TA, δ^{13}C-DIC), solid of total organic matter (TOC), and calcium carbonate ($CaCO_3$) were taken from Wu et al. (2018). Porewater Sr^{2+} concentration was measured by ICP-OES (iCAP 6300 Duo, Thermo Fisher) using 25-fold dilutions (Dellwig et al., 2007). For the determination of extractable Ca, Mg, and Sr of carbonate in the sediment, the freeze-dried samples were leached with 0.5 m HCl at room temperature under continuous agitation for ca. 1 h (Kowalski et al., 2012). Total extraction of the sediment was filtered through 0.45 mm SFCA (Surfactant-Free Cellulose Acetate) syringe filters and was

Page: 8

Number: 1	Subject: Line	Date: 16/07/2022 16:12:46
Number: 2	Subject: Line	Date: 16/07/2022 16:10:55
Number: 3)	Subject: Text Box	Date: 16/07/2022 16:11:30
Number: 4 (	Subject: Text Box	Date: 16/07/2022 16:11:20
Number: 5	Subject: Line	Date: 16/07/2022 16:10:57
Number: 6	Subject: Line	Date: 16/07/2022 16:12:42
Number: 7	Subject: Line	Date: 16/07/2022 16:12:39

measured by ICP-OES (iCAP 6300 Duo, Thermo Fisher). The carbon isotopic compositions of bulk carbonates were analyzed on a Thermo Finnigan MAT 253 isotope ratio mass spectrometer coupled to a Thermo Finnigan Gasbench II using 100 μg powdered samples. The carbon isotopic ratios are reported in the standard δ notation with respect to the VPDB standard and with a precision of better than ±0.1% (1σ), as:

$$\delta^{13}\mathrm{C} - C = \left(\frac{^{13}C/^{12}C}{(^{13}C/^{12}C)_{VPDB}} - 1\right) \cdot 1000 \quad (6)$$

Scanning electron microscopy (SEM) and energy dispersive X-ray microanalyses (EDX) were performed at Leibniz IOW on an FEI Quanta 400 microscope connected to an EDAX-Genesis system.

2.3 Modeling approach

2.3.1 Reactive-transport model

The sampling data from sites SO-8, SO-23, SO-26, SO-45, and SO-50 were simulated with an RTM to quantify the processes controlling porewater SO_4^{2-}, Ca^{2+}, Mg^{2+}, Sr^{2+}, CH_4 (=^{12}C-CH_4 + ^{13}C-CH_4), DIC (=^{12}C-DIC + ^{13}C-DIC) and TA concentrations, and solid $CaCO_3$ and δ^{13}C-$CaCO_3$ in the sediments. The geochemical reactions coupled in the RTM, symbol definitions, and rate of each reaction are listed in Tables 2-4, respectively.

Because of the abundance of sulfate in seawater relative to other terminal electron acceptors (e.g., O_2, NO_3^-, Mn-(hydr)oxides, Fe-(hydr)oxides), microbial respiration coupled to organic matter degradation (*OM*) is primarily driven by organoclastic sulfate reduction (*OSR*) and methanogenesis (ME) (Böttcher et al., 1998; Froelich et al., 1979). Upwardly diffusing CH_4 can be subsequently reoxidized within the sulfate-methane

This page contains no comments

transition zone (SMTZ), where sulfate reduction is coupled to AOM. The AOM and OSR processes facilitate the conversion of organic carbon to DIC and subsequent precipitation of carbonate. Based on these biogeochemical processes mentioned above, depth profiles of the dissolved species and solids were simulated by numerically solving the following mass conservation equation (Berner, 2020; Boudreau, 1997),

$$\varphi(x)\cdot\frac{\partial C_i(x,t)}{\partial t}=\frac{\partial\left(\varphi(x)\cdot\frac{D_i(x)}{\tau^2}\frac{\partial C_i(x,t)}{\partial x}\right)}{\partial x}-\frac{\partial\left(\varphi(x)\cdot v(x)\cdot C_i(x,t)\right)}{\partial x}+\varphi(x)\cdot\sum R(x,t) \quad (7)$$

$$\left(1-\varphi(x)\right)\cdot\frac{\partial C_i(x,t)}{\partial t}=-\frac{\partial\left(\left(1-\varphi(x)\right)\cdot w(x)\cdot C_i(x,t)\right)}{\partial x}+\left(1-\varphi(x)\right)\cdot\sum R(x,t) \quad (8)$$

where x (m) is the depth below seafloor, t (yr) is time, φ is porosity, D_i ($m^2\ yr^{-1}$) is the molecular diffusion coefficient of the dissolved species i, τ^2 is tortuosity calculated as $\tau^2=1-\ln(\varphi^2)$, v ($cm\ yr^{-1}$) is the burial velocity of the dissolved species in the porewater, w ($cm\ yr^{-1}$) is the burial velocity of the solid species, C_i (mM) is the concentration of the dissolved species (mM) or solid content of TOC and $CaCO_3$ (dry weight percent, wt.%) and $\sum R$ is the sum of biogeochemical reaction rates affecting each dissolved species. Simple exponential function was used to describe porosity in sediments:

$$\varphi(x)=\varphi_f+\left(\varphi_0-\varphi_f\right)\cdot e^{-\lambda x} \quad (9)$$

where φ_f and φ_0 are the values of porosity at larger depth and at the sediment-water interface (SWI), respectively, and λ is an attenuation coefficient. Considering sediment compaction, the burial velocities of aqueous ($v(x)$) and the solid phase ($w(x)$) follow the conservation law: $v(x)=w_f\varphi_f/\varphi(x)$ and $w(x)=w_f(1-\varphi_0)/(1-\varphi(x))$, where w_f is the compacted burial velocity of sediment at depth.

A reaction continuum model based on Gamma distribution (γ-RCM) was chosen to describe the degradation of organic matter (Boudreau and Ruddick, 1991). The rate of

Page: 10

Number: 1 Subject: Line Date: 16/07/2022 16:19:52

Number: 2 Subject: Arrow Date: 16/07/2022 16:19:58

Number: 3 Subject: Sticky Note Date: 16/07/2022 16:19:53

you may add Berner 1980.

Number: 4 Subject: Sticky Note Date: 16/07/2022 16:21:21

not uderstandable for a scheintist out of the field.
Why not write:
the concentration of a specie (i) = ...
Ci(x,t) = ...

Number: 5 Subject: Sticky Note Date: 16/07/2022 16:22:28

Here is the beginning of another §.

Number: 6 Subject: Sticky Note Date: 16/07/2022 16:23:20

should we find the numerical values in a table ?

organic matter degradation (R_{OM}, wt.% yr^{-1}) can be written as:

$$R_{\mathrm{OM}}(t) = G(0) \cdot \frac{v_R \cdot a^{v_R}}{(a+t)^{v_R+1}} \tag{10}$$

where $G(0)$ is the concentration of organic matter at the SWI, parameter v_R is the shape parameter, and a represent the initial age of organic matter (Boudreau and Ruddick, 1991).

Considering the exponentially decreasing porosity, the time (t) in the Eq. (10) can be written as (Meister et al., 2019):

$$t(x) = \int_0^x \omega^{-1} dx = \frac{x}{\omega_f} + \frac{(\varphi_0 - \varphi_f)}{(1-\varphi_f) \cdot a \cdot \omega_f} \cdot (e^{-a \cdot x} - 1) \tag{11}$$

The degradation rate of organic matter is stoichiometrically linked to sulfate reduction rate (R_{SR}) and methanogenesis rate (R_{ME}), as:

$$R_{\mathrm{SR}} = f_{\mathrm{C}} \cdot f_{\mathrm{S}} \cdot R_{\mathrm{OM}} \tag{12}$$

$$R_{\mathrm{ME}} = f_{\mathrm{C}} \cdot (1 - f_{\mathrm{S}}) \cdot R_{\mathrm{OM}} \tag{13}$$

where f_C is the factor that converts unit wt.% to mM:

$$f_{\mathrm{C}} = \frac{\rho_{\mathrm{S}} \cdot (1 - \varphi(x)) \cdot 10^4}{M_C \cdot \varphi(x)} \tag{14}$$

where ρ_S is the density of dry sediment, M_C is the molecular weight of carbon. The f_S is a rate-limiting term that determines whether organic matter degradation is attributed to sulfate reduction or methanogenesis, defined using error residual functions (Chuang et al., 2019; Dale et al., 2019):

$$f_{\mathrm{S}} = 0.5 \cdot erfc\left(\frac{[SO_4^{2-}] - C_S^*}{b}\right) \tag{15}$$

where $[SO_4^{2-}]$ is the concentration of sulfate, C_S^* is the threshold sulfate concentration for methanogenesis (~1 mM), and b is a parameter controlling the steepness of f_S (Table 4).

This page contains no comments

The rate of AOM (R_{AOM}) was expressed by bimolecular kinetic function ((Regnier et al., 2011):

$$R_{AOM}=k_{AOM} \cdot [CH_4] \cdot [SO_4^{2-}] \tag{16}$$

where k_{AOM} is the rate constant for AOM, [CH_4] is methane concentration.

2.3.2 Authigenic carbonate precipitation

The precipitation rate of authigenic carbonate (R_{AC}) is related to the saturation state of sedimentary calcium ions (Ω, Eq. (17)) and can be calculated by a linear approximation (Eq. (18)) (Luff et al., 2001).

$$\Omega=\frac{[Ca^{2+}]\cdot[CO_3^{2-}]}{K_{SP}^*} \tag{17}$$

$$R_{AC}=k_{Ca} \cdot (\Omega - 1) \tag{18}$$

where k_{Ca} is the first kinetic rate for authigenic carbonate formation, K_{SP}^* is the stoichiometric solubility constant of solid carbonate, [Ca^{2+}] is the concentration of calcium ions, and [CO_3^{2-}] is the concentration of carbonate. Aragonite and calcite are two main forms of authigenic carbonate minerals (Bayon et al., 2007). The saturation of these two forms of authigenic carbonates is reflected by their stoichiometric solubility constant (K_{SP}^*), which is closely related to the temperature. The temperature in the Beibu Gulf sediment is about 8°C (Cai et al., 2012) and the K_{SP}^* for aragonite and calcite are about 0.74 $mmol^2\ kg^{-2}$ and 0.43 $mmol^2\ kg^{-2}$ at 8°C, respectively (Mucci, 1983; Zeebe and Wolf-Gladrow, 2001). The rate of authigenic carbonate formation can be calculated by combining the formation rates of calcite (R_{cal}) and aragonite (R_{ara}) in the sediments (Berner, 2020; Morse et al., 1997; Mucci, 1983; Schott et al., 2009):

$$R_{AC} = f_{cal}(x) \cdot R_{cal} + f_{ara}(x) \cdot R_{ara} \tag{19}$$

Page: 12

Number: 1 Subject: Sticky Note Date: 16/07/2022 16:24:24

obiously

Number: 2 Subject: Line Date: 16/07/2022 16:24:27

Number: 3 Subject: Sticky Note Date: 16/07/2022 16:24:56

?

Number: 4 Subject: Line Date: 16/07/2022 16:24:44

Number: 5 Subject: Sticky Note Date: 16/07/2022 16:26:24

NO;
The saturation state (Omega) depend in the 3 parameters in your equation (17); not only on [Ca2+]

Number: 6 Subject: Line Date: 16/07/2022 16:24:42

Number: 7 Subject: Sticky Note Date: 16/07/2022 16:27:20

you know how difficult it is to assign a value to the kinetic rate !?
any discution on this later in the article may be.

Number: 8 Subject: Line Date: 16/07/2022 16:26:27

Number: 9 Subject: Line Date: 16/07/2022 16:26:28

Number: 10 Subject: Line Date: 16/07/2022 16:26:31

$$R_{cal} = k_{ca} \cdot (\Omega_{cal} - 1), \quad R_{ara} = k_{ca} \cdot (\Omega_{ara} - 1) \tag{20}$$

where $f_{cal}(x)$ and $f_{ara}(x)$ are the fractions of calcite and aragonite in the authigenic carbonate, Ω_{cal} and Ω_{ara} are their saturation in the porewater. High sulfate concentrations (>20 mM) in surface sediment have previously been considered to prevent the formation of calcite and promote aragonite formation (Aloisi et al., 2002; Mazzini et al., 2006; Peckmann et al., 2001). Calcite, especially high-Mg calcite, is assumed to be easily formed within the SMTZ (Nöthen and Kasten, 2011). Based on the rate of calcite and aragonite formation within different layers in the sediments, we calculated calcite fraction ($f_{cal}(x)$) as follow:

$$f_{cal}(x) = \alpha \cdot \frac{R_{AOM}(x)}{R_{AOM,Maximum}} \tag{21}$$

where $R_{AOM,Maximum}$ is the maximum value of AOM rate, and α ($0 \leq \alpha \leq 1$) is the fraction of calcite at the depth of $R_{AOM,Maximum}$. The fraction of aragonite can be calculated as $f_{ara}(x)=1-f_{cal}(x)$.

The production/consumption rates of DIC and TA in the OSR, AOM, methanogenesis, and authigenic carbonate are shown in Tables 2 and 3. It should be noted that the HS^- produced during the AOM is one component of TA, but not DIC (Middelburg et al., 2020; Zeebe and Wolf-Gladrow, 2001). Based on the porewater profiles of DIC and TA in the study sites, we used CO2SYS (v3.0) to calculate the porewater pH and concentration of carbonate species (Humphreys et al., 2020; Sharp et al., 2020). When carbonate is under saturation state ($\Omega<1$), the dissolution of the authigenic carbonate will occur (Luff et al., 2001). In this study, the carbonate dissolution process could be ignored since carbonate saturation is supersaturated (Wu et al., 2018). The precipitation

Page: 13

Number: 1 Subject: Sticky Note Date: 16/07/2022 16:30:27

is this a result ?
Or a data to be mentionned in the §Environmental Setting ?

anyway, not in this § I think.

Number: 2 Subject: Sticky Note Date: 16/07/2022 16:31:00

quite obioulsy, yes.
Why to you mention that ?

Number: 3 Subject: Sticky Note Date: 16/07/2022 16:33:39

Ok, that is a BIG hypothesis.
I nature, you often have not dissolution/precipitation even when Omega is different from 1; because of kinetic/metastable effects...
Mention explicitely that you take the hypothesis that calcite precipitatio/dissolutioin as soon as Omega is differetn from 1.

Number: 4 Subject: Line Date: 16/07/2022 16:33:41

rate of porewater strontium (Sr^{2+}) is correlated with Ca^{2+} precipitation (Fantle and DePaolo, 2006; Fantle and DePaolo, 2007; Zhang and DePaolo, 2020), and the precipitation rate of Mg^{2+} is correlated with the high Mg-calcite formation (Bayon et al., 2007). Thus, the precipitation rate of Sr^{2+} and Mg^{2+} can be written as:

$$R_{Sr} = K_{Sr} \cdot \frac{C_{Sr}}{C_{Ca}} \cdot R_{AC} \quad , \quad R_{\mathrm{Mg}} = K_{Mg} \cdot \frac{C_{Mg}}{C_{Ca}} \cdot R_{AC} \tag{22}$$

where C_{Sr}, C_{Mg}, and C_{Ca} are the concentration of the porewater Sr^{2+}, Mg^{2+}, and Ca^{2+}, R_{AC} is the formation rate of authigenic calcium carbonate (Eq. 19), K_{Sr} is the equilibrium partition coefficient of Sr^{2+}, K_{Mg} is the equilibrium partition coefficient of Mg^{2+} in high Mg-calcite, and R_{cal} is the formation rate of calcite. Accordingly, the rate of solid authigenic carbonate formation ($R_{\mathrm{AC\_S}}$) can be calculated as:

$$R_{AC\_S} = R_{AC} / f_{Ca} \tag{23}$$

where f_{ca} is the factor of the unit conversion from mM to wt.%, and M_{Ca} is the molecular weight of carbon carbonate.

$$f_{ca} = \frac{\rho_S \cdot (1 - \varphi(x)) \cdot 10^4}{M_{Ca} \cdot \varphi(x)} \tag{24}$$

2.3.3 Stable carbon isotope

The carbon isotope model is based on mass balance equations for ^{13}C-DIC and ^{12}C-DIC. Porewater δ^{13}C-DIC was expressed as the Vienna Peedee Belemnite standard (VPDB) according to Eq. (6) (Brand and Coplen, 2012). The fractionation of carbon isotopes during the sulfate reduction is negligible, with an experimentally determined fractionation factor of about 1 (Londry and Des Marais, 2003; Meister et al., 2019). The rate of DI^{13}C produced by sulfate reduction ($^{13}R_{\mathrm{SR}}$) can be written as (Chuang et al., 2019; Dale et al., 2019):

Page: 14

Number: 1 Subject: Sticky Note Date: 16/07/2022 16:35:00

this sentence means nothing.
You will not precipitatite native Strontium !
(you could precipitate baryte, or Sr riche carboantes...)

Number: 2 Subject: Line Date: 16/07/2022 16:33:44

$$^{13}R_{SR} = \frac{\delta^{13}\mathrm{C-TOC+1000}}{\delta^{13}\mathrm{C-TOC+1000+1000}/(^{13}C/^{12}C)_{VPDB}} \cdot R_{SR} \quad (25)$$

where δ^{13}C-TOC varies from -26‰ to -20‰ in the study area (Wu et al., 2018).

The rate of DI^{13}C produced by AOM ($^{13}R_{\mathrm{AOM}}$) can be described as:

$$^{13}R_{\mathrm{AOM}} = \frac{^{13}CH_4}{\alpha_{\mathrm{AOM}} \cdot CH_4 + {}^{13}CH_4 \cdot (\alpha_{\mathrm{AOM}} - 1)} \cdot R_{\mathrm{AOM}} \quad (26)$$

where the fractionation factor of AOM, α_{AOM}, is between 1.01 and 1.04 (Holler et al., 2009).

The autotrophic pathway is the main form of methanogenesis in sediments (Blair, 1998; Burdige et al., 2016; Whiticar et al., 1986). It is a two-step process in which organic matter is first fermented to CO_2 and H_2, without significant isotopic fractionation, and then followed by a methanogenesis process through CO_2 reduction, which has a significant fractionation of carbon isotope (Jørgensen et al., 2010). The carbon isotope mass balance for organic matter fermentation ($^{13}R_{\mathrm{ferm}}$) and CO_2 reduction to CH_4 ($^{13}R_{\mathrm{ME}}$) can be written as:

$$^{13}R_{\mathrm{ferm}} = \frac{\delta^{13}\mathrm{C-TOC+1000}}{\delta^{13}\mathrm{C-TOC+1000+1000}/(^{13}C/^{12}C)_{VPDB}} \cdot R_{\mathrm{ME}} \quad (27)$$

and

$$^{13}R_{\mathrm{ME}} = \frac{1}{2} \cdot \frac{\mathrm{DI}^{13}\mathrm{C}}{\alpha_{\mathrm{ME}} \cdot \mathrm{DIC} + \mathrm{DI}^{13}\mathrm{C} \cdot (\alpha_{\mathrm{ME}} - 1)} \cdot R_{\mathrm{ME}} \quad (28)$$

where the range of its fractionation factor (α_{ME}) was from 1.02 to 1.06 observed by incubation experiments (Whiticar et al., 1986).

Several studies found the fractionation factor for carbonate precipitation (α_{AC}) is close to 1 (Chuang et al., 2019; Teichert et al., 2005). The rate of ^{13}C-DIC produced by authigenic carbonate formation ($^{13}R_{\mathrm{AC}}$) can be written as:

$$^{13}R_{\mathrm{AC}} = \frac{\mathrm{DI}^{13}\mathrm{C}}{\alpha_{\mathrm{AC}} \cdot \mathrm{DIC} + \mathrm{DI}^{13}\mathrm{C} \cdot (\alpha_{\mathrm{AC}} - 1)} \cdot R_{\mathrm{AC}} \quad (29)$$

This page contains no comments

Marine sediment carbonate is mainly composed of biogenic carbonate (BC) and authigenic carbonate (AC) (Mitnick et al., 2018). Based on the carbon isotope mass balance of sediment carbonate, the carbon isotope of solid carbonate (δ^{13}C-$CaCO_3$) can be calculated as (Mitnick et al., 2018):

$$\delta^{13}C - CaCO_3 = f_{AC}(x) \cdot \delta^{13}C - AC + f_{BC}(x) \cdot \delta^{13}C - BC \quad (30)$$

where $f_{AC}(x)$ and $f_{BC}(x)$ are the fractions of AC and BC, respectively. The δ^{13}C-BC was ~ 0‰(Bayon et al., 2007; Hu and Burdige, 2007). The $f_{AC}(x)$ can be calculated as the ratio between the contents of authigenic carbonate and the solid carbonate:

$$f_{AC}(x) = \frac{C_{AC}(x)}{C_{solid-carbonate}(x)} \quad (31)$$

where C_{AC} and $C_{solid\text{-}carbonate}$ are the content of authigenic carbonate and the measured solid-carbonate in the sediments, respectively.

2.3.4 Boundary conditions, non-steady-state setting, and numerical solution

The values of the upper boundary for SO_4^{2-}, DIC, TA, Ca^{2+}, Mg^{2+}, Sr^{2+}, δ^{13}C-DIC, and δ^{13}C-$CaCO_3$ were determined according to the porewater profiles of sampling sites. The upper boundary of CH_4 and the lower boundary of SO_4^{2-}, DIC, TA, Mg^{2+}, Sr^{2+}, Ca^{2+}, and δ^{13}C-DIC were designated as the Neumann boundary, where the gradients of their concentrations could be assumed to be zero.

Based on the porewater SO_4^{2-} and Ca^{2+} profiles, the sedimentary condition with non-steady-state was observed at sites SO-8, SO-23, and SO-26, which is mainly caused by an increase of underlying methane concentration (Wu et al., 2018). First simulated the steady-state conditions without methane-bearing fluids in the underlying sediments, where the degradation of organic matter occurred only through sulfate reduction, and

Page: 16

Number: 1 Subject: Line Date: 16/07/2022 16:37:30

Number: 2 Subject: Sticky Note Date: 16/07/2022 16:38:25

You could fuse that i 1 sentance to expain that the ocean being an infintie reservoir, you chose Neumann condition at the upper boundary of the model.

Number: 3 Subject: Line Date: 16/07/2022 16:38:47

Number: 4 Subject: Sticky Note Date: 16/07/2022 16:39:24

rephrase

Number: 5 Subject: Sticky Note Date: 16/07/2022 16:39:48

beggening of a new § ?

Number: 6 Subject: Sticky Note Date: 16/07/2022 16:41:24

why you chose this model ? What do you mean you deactive methanogenesis ? R3=0 ?

then simulated the dynamics of AOM and the authigenic carbonate formation in the sediment with time when the underlying methane concentration increased. With the extension of the simulation time, the methane in the sediment is sufficiently consumed with sulfate, and the reaction system eventually reaches a steady-state again. Due to a lack of measured bottom methane data, the lower boundary of methane concentration under the non-steady-state was determined through the simulations of the profiles of SO_4^{2-}, DIC, TA, and δ^{13}C-DIC.

The set of coupled partial differential equations was solved by the finite difference method (FDM) with implicit discretization (Gautschi, 1997). The nonlinear equations were solved by the Newton-iterative method (Gautschi, 1997), and the code was written by Matlab (R2021b). All parameters (e.g., v_R, a, k_{AOM}, K_{SR}, K_{Mg}) were fitted by the least-squares curve-fitting function lsqcurvefit in Matlab based on porewater and sediment profiles. The best-fit parameters and boundary conditions obtained at each site are present in Table 5.

3.Results

The geochemical data at study sites SO-8, SO-23, SO-26, SO-45, and SO-50 containing the depth profiles of porewater (e.g., SO_4^{2-}, Ca^{2+}, Mg^{2+}, Sr^{2+}, DIC, TA), solid sediments (e.g., TOC, $CaCO_3$, and δ^{13}C-$CaCO_3$), and their simulated results are shown in Fig.2 and Fig.3. The geochemical compositions of the porewater and the sediments were described in the previous study (Wu et al., 2018). Based on the porewater SO_4^{2-} concentration gradient in the depth profiles, we categorized site SO-8, SO-23, and SO-

Page: 17

Number: 1 Subject: Sticky Note Date: 16/07/2022 16:41:32

this is a result ?

Number: 2 Subject: Sticky Note Date: 16/07/2022 16:42:42

I am not a specialist of numerical solving, and connot provide a review for this §.

Number: 3 Subject: Sticky Note Date: 16/07/2022 19:29:00

Nothing about you methode to extrapolate the results from you study site to Plant Earth ?
Which methode did you used ?

Number: 4 Subject: Line Date: 16/07/2022 16:42:53

Number: 5 Subject: Sticky Note Date: 16/07/2022 19:02:43

not a result, but part of the description of the samples.

Number: 6 Subject: Sticky Note Date: 16/07/2022 16:43:47

you already mention this in the § 'Study Area', right ? Don't repeat

26 as *Group* I, where complete SO_4^{2-} removal from the porewater and much steeper sulfate gradient were observed. The other two sites, SO-45 and SO-50 were classified as *Group* II. In *Group* II, porewater SO_4^{2-} concentrations initially decrease gradually and then stay almost constant vertically with the depth increasing.

3.1 *Group* I sites

The γ-RCM was used to simulate organic matter degradation in our study sites. The heterogeneous organic matter reactivities in Group I are reflected by the difference in parameter *a* (*a*=1324 yr at SO-8, *a*=2831 yr at SO-26, and *a*=4315 at SO-23, Table 5) that the smaller the value of *a*, the higher the organic matter reactivity (Arndt et al., 2013). The difference in parameter *a* at the different sites indicates the complex depositional environment in the Beibu Gulf. By integrating the rate per unit volume of sediment over depth from the seafloor to a prescribed depth in the sediment profiles, we obtained the depth-integrated rates of organic matter degradation that 0.29 mol m^{-2} yr^{-1} at site SO-8, 0.14 mol m^{-2} yr^{-1} at site SO-23, and 0.24 mol m^{-2} yr^{-1} at site SO-26, respectively.

The profiles of SO_4^{2-} show a concave-up trend in *Group* I, which is due to the upward shift of the SMTZ caused by the higher underlying CH_4 fluxes (Table 5) (Blouet et al., 2021; Regnier et al., 2011). This can be further confirmed by the higher AOM rates shown in Fig. 4. By calculating the depth–integrated rates of OSR and AOM in *Group* I (Table 6), we found the proportions of total sulfate reduction via AOM are ~87% at site SO-23, ~69% at site SO-26, 43% at site SO-8 (Table 6). According to the porewater profiles of DIC and TA, we calculated the porewater pH on the basis of acid-base

Page: 18

Number: 1 Subject: Sticky Note Date: 16/07/2022 19:03:50

Real COMPLETE removal means that you have a infinit gradient, indeed: a step !
be realistic. You don't have complete removal exactly at the sea floor, but at X cm below the sea floor.

Number: 2 Subject: Line Date: 16/07/2022 16:44:24

Number: 3 Subject: Line Date: 16/07/2022 16:44:23

Number: 4 Subject: Sticky Note Date: 16/07/2022 16:46:26

thill a given depth x

Number: 5 Subject: Line Date: 16/07/2022 16:46:29

Number: 6 Subject: Sticky Note Date: 16/07/2022 16:47:42

Re-structure your introduction of group 1 and 2: say: "we observe 2 beahavior, and consequantly descided to analyse the observation in 2 groups"

Number: 7 Subject: Sticky Note Date: 16/07/2022 16:48:06

it is not YOUR study site: it belongs to everybody.

Number: 8 Subject: Line Date: 16/07/2022 16:47:44

Number: 9 Subject: Line Date: 16/07/2022 16:47:46

Number: 10 Subject: Sticky Note Date: 16/07/2022 19:04:41

descripiton of the methode of modeling; not the result.

Number: 11 Subject: Sticky Note Date: 16/07/2022 16:56:20

?

Number: 12 Subject: Sticky Note Date: 16/07/2022 19:06:19

start to defin group 1.

equilibrium system. The calculation results display that pH decreases within the surface layer (~8.1 to ~7.8), increases slightly within the SMTZ (~7.8 to ~8.0), and decreases below the SMTZ (~8.0 to ~7.7) (Fig. 2C). As shown in Fig. 2D, Ca^{2+} concentrations show a decreasing trend in the depth profiles, which indicates the carbonate precipitation occurring in *Group* I. The location of the maximum rate of authigenic carbonate formation is almost consistent with the peak rate of AOM within SMTZ (Fig. 4). The maximum rate of AOM, the maximum rate of authigenic carbonate formation, and the depth–integrated carbonate formation rate (TR_{AC}) at sites SO-23 and SO-26 are similar and approximately 0.15 mol m^{-2} yr^{-1}, 0.008 mol m^{-2} $yr^{-1}$and 0.04 mol m^{-2} yr^{-1}, respectively, significantly higher than those at site SO-8 with the maximum rate of AOM (0.03 mol m^{-2} yr^{-1}), the maximum rate of authigenic carbonate formation (0.0008 mol m^{-2} yr^{-1}), and the TR_{AC} (0.01 mol m^{-2} yr^{-1}). The solid authigenic carbonates accumulated at the bottom of sediments at site SO-23 (~0.35 wt.%) and site SO-26 (~0.39 wt.%) are higher than those at site SO-8 (~0.21 wt.%). All the porewater profiles of Sr^{2+} and Mg^{2+} concentrations show a decreasing trend with the increase of depth in *Group* I site (Fig. 2), indicating their co-precipitation during the authigenic carbonate formation.

The minimum simulated δ^{13}C-DIC values within the SMTZ are around -22‰, -26‰, and -24‰ at site SO-8, SO-23, and SO-26, respectively. Below the SMTZ, the δ^{13}C-DIC becomes heavier due to methanogenesis. The carbon source for authigenic carbonate formation is derived from ambient porewater DIC, which results in the variation trends of the δ^{13}C-AC and δ^{13}C-DIC profiles (Fig. 2). By fitting the results of

Page: 19

Number: 1 Subject: Sticky Note Date: 16/07/2022 19:14:59

not show in your tables...

Number: 2 Subject: Sticky Note Date: 16/07/2022 19:16:25

can you describe more: waht do you mean by 'almost' ?
Also, can you explain this result ?

Number: 3 Subject: Sticky Note Date: 16/07/2022 19:17:16

might worth to expres in mmol

Number: 4 Subject: Line Date: 16/07/2022 19:17:49

Number: 5 Subject: Sticky Note Date: 16/07/2022 19:18:52

it migh worth to add titels of sub§; so the structure of your explanation will aprear more clearly.

δ^{13}C-$CaCO_3$ (Fig. 2), the average percentages of authigenic carbonate in total solid sediment carbonate were calculated as 8.9% (SO-8), 3.1% (SO-23), and 2.2% (SO-26), respectively.

3.2 *Group* II

Compared with Group I, the variation characteristics of the porewater sulfate profile reveal that there is no obvious upward CH_4 flux from the lower boundary and AOM process occurring in Group II. Thus, OSR and production of DIC and TA are controlled directly by organic matter in *Group* II sediments. The higher organic matter reactivity occurs at site SO-45 than at SO-50, which is confirmed by the value of parameter a (a=2419 yr at site SO-45 and a=3410 yr at site SO-50). The depth–integrated rates of organic matter degradation and OSR in *Group* II are TR_{OM}=0.29 mol m^{-2} yr^{-1}, TR_{OSR}=0.14 mol m^{-2} yr^{-1} at SO-45, and TR_{OM}=0.12 mol m^{-2} yr^{-1}, TR_{OSR}=0.06 mol m^{-2} yr^{-1} at SO-50, respectively. The pH profile decreases from ~8.1 at the SWI to ~7.2 at the bottom sediment (Fig. 3C). Similar to *Group* I, the saturation state of authigenic carbonates is also supersaturated in *Group* II (Fig.3D). The depth–integrated rates of authigenic carbonate formation (TR_{AC}) in the *Group* II are TR_{AC}=0.0026 mol m^{-2} yr^{-1} at SO-45 and TR_{AC}=0.0022 mol m^{-2} yr^{-1} in SO-50, respectively, significantly smaller than that in the *Group* I by an order of magnitude (Table 6). The amount of solid authigenic carbonates was calculated to be approximately 0.11 wt.% at SO-45, and 0.08 wt.% at SO-50, and the values were smaller than those in *Group* I. Both δ^{13}C-DIC and δ^{13}C-AC decrease with depth and reach ~-14‰ and ~-13‰ at the bottom of the sediments (Fig. 3G and H). Due to no occurrence of AOM, the percentages of authigenic carbonate in

Page: 20

Number: 1 Subject: Sticky Note Date: 16/07/2022 19:19:12

boring description of what we can see on the graphs.

Number: 2 Subject: Sticky Note Date: 16/07/2022 19:22:05

No; before comparing, start to define and describe Group 2 for waht it is. One described, you can compare.

total sediment carbonate are 1.1% at site SO-45 and 1.2% at site SO-50, which is obviously smaller than that at *Group* I.

3.3 Validation of model based on porewater Sr^{2+} profiles

The formation of authigenic carbonate is accompanied by the precipitation of porewater Sr^{2+} (Charlou et al., 2004; Sosdian et al., 2012). Comparing the ratio of porewater Sr^{2+}/Ca^{2+} and calcium carbonate, the empirical partition coefficient of Sr^{2+} (K_{Sr}) can be estimated at different sites (Fantle and DePaolo, 2006; Fantle and DePaolo, 2007), which could be used to validate the model that we established.

The equilibrium value of K_{Sr} can be calculated theoretically (Böttcher and Dietzel, 2010) or by an empirical formula Eq. (32) with a temperature range from 0 °C to 100 °C (Zhang and DePaolo, 2020).

$$K_{Sr}(T) = 0.025 \cdot \exp\left(\frac{G_r}{R}\left(\frac{1}{298.15} - \frac{1}{T}\right)\right) \tag{32}$$

where G_r is the Gibbs free energy change associated with the exchange reaction (~1.2 Kcal/mol), R is the gas constant (~8.3 J mol^{-1} K^{-1}), T is the temperature (K), and uncertainty is approximately ±20% (Zhang and DePaolo, 2020). As the average temperature in the bottom water of the Beibu Gulf is around 8 °C (Cai et al., 2012), the corresponding K_{Sr} value calculated by Eq. (32) is 0.025 (range: 0.02–0.03). The best-fitting results of K_{Sr} in *Group* I and the *Group* II sites are close to the theoretical value (Table 7), validating the effectiveness of the model that we established.

4. Discussion

4.1 Types of authigenic carbonate formation

This page contains no comments

The Sr/Ca and Mg/Ca in solid sediment are commonly used to distinguish the type of authigenic carbonate (Fig. 5B) (Bayon et al., 2007; Stoll and Schrag, 2000). For example, higher Sr/Ca (~0.027) and lower Mg/Ca (~0.0005) in sediment indicate that more aragonite is formed in the sediments (Naehr et al., 2000). In this study, the lower Sr/Ca (~0.003) and higher Mg/Ca (~0.17) were observed within the SMTZ in *Group* I (sites SO-8, SO-23, and SO-26), which was consistent with the formation of high Mg-calcite (Lear et al., 2002; Rickaby et al., 2002; Rosenthal et al., 1997). Compared to the *Group* I, higher solid Mg/Ca (~0.5) and similar Sr/Ca (~0.004) were found in the *Group* II (Fig. S1-S5 in the Supplementary Information), which indicates little dolomite was formed in the sediments (Bayon et al., 2007; Rodriguez et al., 2000). It should be emphasized that no chemical leaching from substantial clay minerals occurred in our study sites, which is confirmed by the ratios of Sr/Ca and Mg/Ca in sediment (Fig.5B), as well as solid Al profiles (Fig. S1-S5 in the Supplementary Information).

In addition, variations in porewater Ca^{2+}, Mg^{2+}, and Sr^{2+} concentrations can also be utilized to identify the types of carbonate minerals formation in the sediments (Bayon et al., 2007; Fantle and DePaolo, 2006; Nöthen and Kasten, 2011). An increase of porewater Sr^{2+}/Ca^{2+} ratio indicates the formation of a carbonate mineral phase is most likely high Mg-calcite with a low Sr^{2+}/Ca^{2+} ratio. Similarly, an increase in the Mg^{2+}/Ca^{2+} ratio in porewater reveals the precipitation of aragonite, a carbonate mineral phase with a low Mg^{2+}/Ca^{2+} ratio (Bayon et al., 2007). Based on the stoichiometric relationship, two bold lines in Fig. 5A indicate the formation of aragonite and high Mg-calcite. Using the method mentioned in Nöthen and Kasten (2011), we estimated that

This page contains no comments

aragonite in the authigenic carbonate formation in *Group* I accounted for 30% and high Mg-calcite for 70%. Among them, high Mg-calcite was mainly formed within the SMTZ (Fig. 5A), which was further evidenced by Elemental analysis of the selected minerals using an electron microscopy energy spectrometer (Fig. 5C). However, these methods can only be used to estimate the total amount of authigenic carbonate formation in the entire sediments and cannot be used to describe the distribution of aragonite and high Mg-calcite formation at different depths of the sediments.

Based on the distribution characteristics that high Mg-calcite formation is favored in the SMTZ while aragonite is mainly formed in the surface sediments, we further simulated the effect of calcite and aragonite formation in sediments on the porewater Sr^{2+}/Ca^{2+} and Mg^{2+}/Ca^{2+} ratios by parametric sensitivity analysis of the formation ratio of high Mg-calcite and aragonite (($f_{cal}(x)$ and $f_{ara}(x)$ in the Eq. (19)). Our results indicate the occurrence of higher Sr^{2+}/Ca^{2+} and Mg^{2+}/Ca^{2+} ratios caused by the formation of calcite within the SMTZ. Specifically, when the formation of high Mg-calcite in the SMTZ accounts for 90%, the ratios of porewater Mg^{2+}/Ca^{2+} and Sr^{2+}/Ca^{2+} are 32 and 0.03, respectively. Moreover, their ratios will drop sharply to 8 and 0.01 when the formation of high Mg-calcite in the SMTZ is reduced to 50%. During the formation of high Mg-calcite, almost all Ca^{2+} are removed from the porewater while the Mg^{2+} still remains ~40 mM in the SMTZ (Fig. 6A), resulting in a high Mg^{2+}/Ca^{2+} in this sedimentary layer. On the contrary, when there is no AOM reaction in the sediment, the Ca^{2+} concentration (~5 mM), Mg^{2+} concentration (~50 mM), and a lower ratio Mg^{2+}/Ca^{2+}(~10) will appear in the bottom sediments.

This page contains no comments

By combining the formation rates of calcite (R_{cal}) and aragonite (R_{ara}) in the sediments, we also calculated the ratio of the total amount of high Mg-calcite and aragonite in the sediments (Fig.4). Although aragonite is the dominant form of authigenic carbonate outside the SMTZ, the rate of authigenic carbonate formation within the SMTZ is much higher than in other layers. Based on parametric sensitivity analysis of the formation ratio of high Mg-calcite and aragonite, we conclude that 80% of the authigenic carbonates formation at site SO-23 is high-Mg calcite, and 90% of them is formed within the SMTZ.

4.2 Authigenic carbonate formation under non-steady-state condition

4.2.1 The relationship between AOM and authigenic carbonate formation

The formation of non-steady-state conditions is caused by an increase of methane flux at the lower boundary, which not only leads to the upward shift of SMTZ towards the SWI (Fig. 7A and C) (Dale et al., 2008; Meister et al., 2013), but also significantly affects authigenic carbonates formation, as the synchronous peak of both rates of authigenic carbonates and the AOM (Fig.7C). In addition, the AOM reaction significantly intensified the formation of authigenic carbonates in the sediments. The authigenic carbonates formation rate increases dramatically with the increase of the bottom methane, especially at the initial stage of the bottom methane emerging. Specifically, the formation rate of authigenic carbonates in the sediments is only ~0.003 mol m^{-2} yr^{-1} at the time of 1 year after the occurrence of methane diffusion, the rate, however, increases sharply to ~0.012 mol m^{-2} yr^{-1} and ~0.02 mol m^{-2} yr^{-1} at the time of 20 years and 50 years, respectively, and finally reaches a constant level (~0.0354 mol

This page contains no comments

m^{-2} yr^{-1}) at the time of 400 years after methane diffusion (Figs.7 and 8). By comparison, we further found that the non-steady-state has a greater impact on the AOM than authigenic carbonate formation, as evidenced by the larger gradient in AOM rate (Fig. 8A) and the almost one order of magnitude higher rate of final AOM (~0.133 mol m^{-2} yr^{-1}) than that of the authigenic carbonate formation. In addition, up to 80% of the authigenic carbonate formation is attributed to AOM by combining the simulated data of carbonate formation rates with and without methane diffusing from the bottom sediments of site SO-23 (Fig. 8B).

The rates of authigenic carbonate formation within the SMTZ in this study area are significantly higher than in other regions (Fig. 7C) (Blouet et al., 2021; Luff et al., 2005). Previous studies have revealed that AOM governs authigenic carbonates formation in the sediments of the marine continental shelf, where enrichment of organic carbon in sediments leads to a strong methanogenic process occurring at the bottom and even formation of methane hydrate (Blouet et al., 2021; Luff and Wallmann, 2003). Mitnick et al. (2018) observed high rates of authigenic carbonate formation by simulating porewater profiles data (e.g., Ca^{2+}, SO_4^{2-}, Sr^{2+}) from sites in the International Ocean Discovery Program (IODP) databases under steady-state conditions and explained that it was caused by the strong sulfate reduction and high sedimentation rate. Based on existing relevant data from continental margin sites, we estimated their SMTZ depths and the associated CH_4 fluxes into the SMTZ (Table 8). Assuming that AOM in the SMTZ is the main process of methane consumption, we obtained a well log-log linear regression relationship between AOM and authigenic carbonate formation after

This page contains no comments

replacing the depth-integrated AOM rate with the CH_4 flux into the SMTZ under a steady-state and (Fig. 8B), which well reflected that the authigenic carbonate formation was substantially promoted by AOM. According to the confidence bounds of the linear regression (two red dashed curves in Fig. 8B), we further plotted their possible relationship on a larger scale. Comparing our study sites with the those listed in Table 8, it can be inferred that the occurrence of shallower SMTZ depth and higher CH_4 flux into the SMTZ are affected by the non-steady-state condition, resulting in higher rates of AOM and authigenic carbonate formation. Furthermore, the relationship between the rates of AOM and authigenic carbonate formation rapidly converged to the empirical formula with the upward of underlying methane, i.e., their rates at the time of ~50 years after the occurrence of methane diffusion were in the confidence bounds and quite close to the empirical formula when they eventually reached the steady-state condition (Fig. 8B). Considering CH_4 flux into the SMTZ decreases exponentially with depth, the ratio of authigenic carbonate formation and AOM rate under the non-steady-state is higher than that in a larger dataset with a wider range of the SMTZ depth (Fig. 8B).

The influence of AOM on the authigenic carbonate formation within the SMTZ is mainly controlled by DIC and alkalinity generated by AOM (Berner, 2020; Luff and Wallmann, 2003; Sun and Turchyn, 2014; Wallmann et al., 2012). Since hydrogen sulfide (HS^-) produced by AOM is a component of TA rather than DIC (Eq. (6)), the production rate of TA is higher than DIC, which causes an increase in porewater pH and promotes the precipitation of carbonate (Zeebe and Wolf-Gladrow, 2001). Hence, the formation of authigenic carbonates in sediments is susceptible to the occurrence of

This page contains no comments

AOM (Blouet et al., 2021; Luff and Wallmann, 2003; Nöthen and Kasten, 2011). Our parametric sensitivity analysis of the underlying methane flux (Fig.9) indicates that the higher the CH_4 flux into the SMTZ can lead to the shallower SMTZ occurring in the sediments. Since higher methane diffusion flux can increase the reaction rate of AOM, it thus becomes the other factor regulating the authigenic carbonate formation in the sediments (Dale et al., 2008; Meister et al., 2013). As shown in Fig. 9, our simulations further reveal that the rate of authigenic carbonate formation is sensitive to the change in methane diffusion flux-when methane diffusion flux increases by 40% (0.049 → 0.069 mM m^{-2} d^{-1}), the rate of authigenic carbonate formation increases by~18% (0.0403 → 0.0476 mM yr^{-1}).

4.2.2 The impact of authigenic carbonate formation on solid δ^{13}C-$CaCO_3$

As discussed above, higher CH_4 flux into the SMTZ induced by the non-steady-state condition can result in higher AOM and authigenic carbonate formation rate. The amount of authigenic carbonate formation caused by the non-steady-state process increased from ~0.1 wt.% in the initial time (1 yr) to ~0.45 wt.% in the final steady-state (400 yr) (Fig. 7D). Meanwhile, the non-steady-state process also causes the change in distribution profiles of δ^{13}C-DIC and δ^{13}C of authigenic carbonate (δ^{13}C-AC) in the sediments, and the positions of the minimum values of both δ^{13}C (DIC and AC) vary synchronously with the upward shift of SMTZ (Fig. 7E). These tendencies of change can be explained by the fact that AOM produced lighter carbon isotopes of DIC and its resulting lighter carbon isotopes of precipitated authigenic carbonates. Since the δ^{13}C-

This page contains no comments

AC is obviously lighter than that of biogenic carbonate (δ^{13}C-BC), the addition of authigenic carbonate to the sediments also makes the δ^{13}C composition of total carbonate (δ^{13}C-$CaCO_3$) lighter in the sediments, especially within the SMTZ (Fig. 7F). Previous studies showed that the fraction of authigenic carbonate in total solid carbonate in continental margin sediments was relatively small. Only if the fraction of authigenic carbonate is greater than 10%, it will have a significant impact on the δ^{13}C-$CaCO_3$ in sediments (e.g., Mitnick et al., 2018). Our sensitivity analysis shows that when the CH_4 flux into the SMTZ is enhanced by 40% (0.049 → 0.069 mM m^{-2} d^{-1}), the authigenic carbonate precipitation in the bottom sediment is increased by 14% (0.37 → 0.42 wt.%, f_{AC}: ~5 → ~6%). Especially in the SMTZ, the fraction of authigenic carbonate in total solid carbonate increased from 3.1% to 5.4%, and the carbon isotope of total solid carbonate (δ^{13}C-$CaCO_3$) varied accordingly from -1‰ to -2‰ (Fig. 9G). Mitnick et al.(2018) assessed the fraction of authigenic carbonate in the sediment by the depth–integrated rate of authigenic carbonate formation and biogenic carbonate flux. By comparing the fractions of authigenic carbonates using the Mitnick et al.(2018)'s model and our established model (Eq. 31), similar results were obtained at sites SO-23, SO-26, SO-45, and SO-50 (Table 9). Considering the difference in the formation rate of authigenic carbonate in different layers, the authigenic carbonate content is obviously different from the surface to the bottom of the sediment, resulting in the uneven fraction of authigenic carbonate in the depth profile of the sediments. For example, the fraction of authigenic carbonate is ~0% on the surface and ~7% at the bottom layer for the site SO-23 (Fig. 9F). However, the method provided by Mitnick et

This page contains no comments

al. (2018) can not reflect the feature of uneven authigenic carbonate formation distribution.

4.2.3 The role of porewater freshening on authigenic carbonate formation

Below the depth of 400 cm in the sediments, a terrestrial sedimentary layer was identified from the lithological characteristics and geochemical profiles of the site SO-8 (Wu et al., 2018), which probably formed in an estuarine or fluvial environment before the Holocene transgression occurred in 12–11.5 cal. ka BP (Li et al., 2010). Due to a deep supply of low-salinity freshwater to the overlying sediments of this site, porewater Cl^- concentration decreased from 530 mM at 400 cm depth to 450 mM at 720 cm depth in the sediments (Fig. 10A). The carbonate content, correspondingly, changed dramatically within the terrestrial sedimentary layer (9 → 2 wt.%) (Fig. 10A). These features indicated that porewater freshening has a great influence on the formation of authigenic carbonate and solid carbonate isotopes.

The salinity transition is commonly observed in shallow boreholes close to the trench at subduction zones (Bekins et al., 1995; Kastner et al., 1991; Saffer and Bekins, 1998; Saffer and McKiernan, 2009), and the porewater freshening will certainly increase the gradient of dissolved chemical species. In order to eliminate this effect, we used porewater Cl^- concentrations for correction ($C_i^{corr} = C_i(x)/(Cl^-(x)/Cl^-(0))$, where $Cl^-(0)$ is the Cl^- concentration at the SWI) (Mitnick et al., 2018). Given the advection and diffusion are the main factors affecting the distribution of porewater Cl^- in the sediments (Aloisi et al., 2015; Ni et al., 2020; Soulet et al., 2010), a two-end-member model was utilized to simulate Cl^- profile at site SO-8, namely Cl^- concentration was 450 mM

This page contains no comments

below 400 cm and 530 mM above 400 cm, respectively (Fig. 10A). The modeling results showed that the increase of salinity could promote the rate of authigenic carbonates formation in sediments because of lager Ca^{2+} fluxes as supplied by salty seawater (Fig. 10C). Although the rate of authigenic carbonates formation in the terrestrial sediment layer is low (0.0089 → 0.0051 mol m^{-2} yr^{-1}), it still has a profound effect on the carbonate isotope composition especially in the bottom sediments, up to 14.5% (Fig. 10D), and this value is significantly higher than that of marine sediments at other sites (Table 9).

In addition, the authigenic carbonate fraction at site SO-8 calculated by the method of Mitnick et al. (2018) was ~1.9%, and the value of δ^{13}C-$CaCO_3$ is ~-5‰. On the basis of isotopic mass balance, if δ^{13}C-BC is around 0‰, the value of δ^{13}C-AC will reach an incredible value of ~-260‰. On the contrary, our modeling results showed that the total fraction of authigenic carbonate in sediment was about 8.9% (Fig. 10). Such higher fraction of authigenic carbonate in the bottom of site SO-8 is caused by the porewater freshening, resulting in a smaller content of carbonate in the terrestrial layer than in the marine layer. Moreover, if we assume carbonate content is relatively constant with a value of ~9 wt.% above the terrestrial- marine transition and ~2 wt.% below this transition at the site SO-8, similar results of the authigenic carbonate fraction could be obtained using both methods of Mitnick et al. (2018) and our model. The above comparisons demonstrate that our modeling approach is suitable for calculating the fraction of authigenic carbonate under a complex depositional environment, while the method provided by Mitnick et al. (2018) can only be applied to steady-state conditions

This page contains no comments

with slight variation in carbonate contents.

4.3 Global budget of authigenic carbonate formation.

Authigenic carbonates are considered the third major carbon pool in marine sediments (Mitnick et al., 2018; Schrag et al., 2013). The global authigenic carbonate formation budget in marine sediment ranges from 0.14 Tmol yr^{-1} to 3.6 Tmol yr^{-1} based on different methods (Akam et al., 2020; Bradbury and Turchyn, 2019; Sun and Turchyn, 2014; Wallmann et al., 2008). For example, Akam et al. (2020) estimated the rate of authigenic carbonate formation was ~1.7 Tmol yr^{-1} on the basis of stoichiometric relationships of AOM, which was close to the estimation by Sun et al. (2014) (~1.0 Tmol yr^{-1}) and Wallmann et al. (2008) (~1.5 Tmol yr^{-1}). Meanwhile, an estimated ~2.8 Tmol of CH_4 was consumed annually within the SMTZ, with 80% occurring in continental sediments (Egger et al., 2018). According to the global CH_4 flux provided by Egger et al. (2018) and the established relationship between AOM and authigenic carbonate formation (Fig. 8B), we further estimate that ~0.49 Tmol yr^{-1} of authigenic carbonates is formed in global marine sediments, with 67% of it occurring in continental shelf sediments (Table 10). The total global carbonate burial is approximately 32 Tmol yr^{-1} in marine sediments (Bradbury and Turchyn, 2019; Lerman et al., 2007). Thus, our estimation of authigenic carbonate formation (~0.49 Tmol yr^{-1}) accounts for only about 2% of the total global carbonate deposition, smaller than that estimated by Sun et al. (2014) (~10%), which ignored the impact of biogeochemical reactions and porewater diffusion and advection on authigenic carbonate formation. Nevertheless, we found that slight variations in authigenic carbonate content in

Page: 31

Number: 1 Subject: Line Date: 16/07/2022 19:22:03

Number: 2 Subject: Sticky Note Date: 16/07/2022 19:22:15

introdution, not discussion.

Number: 3 Subject: Sticky Note Date: 16/07/2022 19:32:54

how you make this global estimation ???
You think you can extrapolate the linear regretion observed locally in any environment ?
Each environment have specific boundary condition... how could you extrapolates your results globaly; this is not explained at all !

Number: 4 Subject: Line Date: 16/07/2022 19:22:50

Number: 5 Subject: Line Date: 16/07/2022 19:30:14

sediments can still significantly impact sediment carbonate isotopes, highlighting that the influence of authigenic carbonates should be fully considered when using carbon isotopes of carbonate to trace paleoceanography in geological history (Bradbury and Turchyn, 2019; Schrag et al., 2013).

5. Conclusion

Porewater and solid sediment geochemical profiles in the Beibu Gulf, South China Sea have been utilized to investigate the role of AOM on the authigenic carbonate formation and its carbon isotopic composition under a non-steady-state by a reactive-transport modeling approach. Authigenic carbonate formation rate is ~0.035 mmol m^{-2} yr^{-1} in *Group* I (SO-8, SO-23, and SO-26), an order of magnitude higher than that in *Group* II (~0.0026 mmol m^{-2} yr^{-1}). Meanwhile, the synchronous peaks of both rates of authigenic carbonates and the AOM occur within the SMTZ, revealing that the AOM can significantly promote authigenic carbonate formation. The lower Sr/Ca (~0.003) and higher Mg/Ca (~0.17) are shown within the SMTZ at *Group* I, which was consistent with the removal of almost porewater Ca^{2+} and formation of high Mg-calcite. By combining the formation rates of calcite (R_{cal}) and aragonite (R_{ara}) in the sediments, we calculated the ratio of the total amount of high Mg-calcite and aragonite in the sediments.

The non-steady-state caused by an increased methane flux in the bottom sediments not only results in the upward shift of the SMTZ but also intensifies AOM and authigenic carbonates formation, particularly in the early stage of methane occurrence. Since AOM produces lighter carbon isotopes of DIC and the associated authigenic carbonates, the

This page contains no comments

burial of authigenic carbonate significantly impacts carbonate isotopes, with even a 14% increase in authigenic carbonate accumulated in sediments resulting in a shift in sediment carbonate isotopes from -1‰ to -2‰. Moreover, the terrestrial- marine transition was found at site SO-8, and our modeling revealed that porewater freshening strongly impacts the formation of authigenic carbonate and carbonate isotopes.

Based on our obtained relationship between the rates of AOM and authigenic carbonate formation, we estimated ~0.49 Tmol yr^{-1} of methane-derived authigenic carbonates burial in global marine sediments. In the future, more relevant geochemical data from the global marine sediments should be collected and compiled to establish a more accurate relationship between the rates of authigenic carbonate formation and AOM and to further explore the contribution of authigenic carbonate formation in marine sediments to the global carbon cycle.

6. Acknowledge

We acknowledge financial support from the German Ministry for Education and Research (BMBF) through contract number 03F0607A and Leibniz IOW. We further thank the master, crew, and participants of RV Sonne for their support during sampling on board. This study was further supported by the National Key Basic Research and Development Program of China (2016YFA0601100) and the Natural Science Foundation of China (41976057). Bo Liu acknowledges additional funding from the Helmholtz Association (Alfred Wegener Institute Helmholtz Centre for Polar and Marine Research).

This page contains no comments

Appendix A. Supplementary Material

Five figures and one data table are included in the Supplementary Materials: Figs. S1-S5, solid Ca, Mg, Sr, Al profiles at our study sites. Table S1, solid Ca, Mg, Sr, Al data.

References

Akam, S.A., Coffin, R.B., Abdulla, H.A., Lyons, T.W., 2020. Dissolved inorganic carbon pump in methane-charged shallow marine sediments: state of the art and new model perspectives. Frontiers in Marine Science, 7: 206.

Aloisi, G. et al., 2002. CH4-consuming microorganisms and the formation of carbonate crusts at cold seeps. Earth and Planetary Science Letters, 203(1): 195-203.

Aloisi, G. et al., 2015. Freshening of the Marmara Sea prior to its post-glacial reconnection to the Mediterranean Sea. Earth and Planetary Science Letters, 413: 176-185.

Arndt, S. et al., 2013. Quantifying the degradation of organic matter in marine sediments: a review and synthesis. Earth-science reviews, 123: 53-86.

Bauer, A. et al., 2013. Regional differences of hydrographical and sedimentological properties in the Beibu Gulf, South China Sea. Journal of Coastal Research(66 (10066)): 49-71.

Bayon, G. et al., 2007. Sr/Ca and Mg/Ca ratios in Niger Delta sediments: implications for authigenic carbonate genesis in cold seep environments. Marine Geology, 241(1-4): 93-109.

Bekins, B.A., McCaffrey, A.M., Dreiss, S.J., 1995. Episodic and constant flow models for the origin of low- chloride waters in a modern accretionary complex. Water Resources Research, 31(12): 3205-3215.

Berner, R.A., 2020. Early diagenesis. Princeton University Press.

Blair, N., 1998. The δ13C of biogenic methane in marine sediments: the influence of Corg deposition rate. Chemical geology, 152(1-2): 139-150.

Blouet, J.-P., Arndt, S., Imbert, P., Regnier, P., 2021. Are seep carbonates quantitative proxies of CH4 leakage?: Modeling the influence of sulfate reduction and anaerobic oxidation of methane on pH and CaCO3 saturation. Chemical Geology: 120254.

Böttcher, M.E., Dietzel, M., 2010. Metal-ion partitioning during low-temperature precipitation and dissolution of anhydrous carbonates and sulphates. European Mineralogical Union Notes in Mineralogy, 10(1): 139-187.

Böttcher, M.E., Oelschläger, B., Höpner, T., Brumsack, H.-J., Rullkötter, J., 1998. Sulfate reduction related to the early diagenetic degradation of organic matter and “black spot” formation in tidal sandflats of the German Wadden Sea (southern North Sea): stable isotope (13C, 34S, 18O) and other geochemical results. Organic Geochemistry, 29(5-7): 1517-1530.

Boudreau, B.P., 1996. A method-of-lines code for carbon and nutrient diagenesis in aquatic sediments. Computers & Geosciences, 22(5): 479-496.

Boudreau, B.P., 1997. Diagenetic models and their implementation, 410. Springer, Berlin.

Boudreau, B.P., Ruddick, B.R., 1991. On a reactive continuum representation of organic matter diagenesis. American Journal of Science, 291(5): 507-538.

Bradbury, H.J., Turchyn, A.V., 2019. Reevaluating the carbon sink due to sedimentary carbonate formation in modern marine sediments. Earth and Planetary Science Letters, 519: 40-49.

This page contains no comments

Brand, U., Veizer, J., 1980. Chemical diagenesis of a multicomponent carbonate system; 1, Trace elements. Journal of Sedimentary Research, 50(4): 1219-1236.

Brand, W.A., Coplen, T.B., 2012. Stable isotope deltas: tiny, yet robust signatures in nature. Isotopes in environmental and health studies, 48(3): 393-409.

Buffett, B., Archer, D., 2004. Global inventory of methane clathrate: sensitivity to changes in the deep ocean. Earth and Planetary Science Letters, 227(3-4): 185-199.

Burdige, D.J., Komada, T., Magen, C., Chanton, J.P., 2016. Methane dynamics in Santa Barbara Basin (USA) sediments as examined with a reaction-transport model. Journal of Marine Research, 74: 277-313.

Cai, L., Fu, S., Yang, J., Zhou, X., 2012. Distribution of meiofaunal abundance in relation to environmental factors in Beibu Gulf, South China Sea. Acta Oceanologica Sinica, 31(6): 92-103.

Charlou, J. et al., 2004. Physical and chemical characterization of gas hydrates and associated methane plumes in the Congo–Angola Basin. Chemical Geology, 205(3-4): 405-425.

Chen, L., Zhang, X., 1986. Mineral assemblages and their distribution pattern of the sediments from the Beibu Gulf. Acta Oceanologica Sinica, 8(3): 340-346.

Chuang, P.-C. et al., 2019. Carbon isotope exchange during anaerobic oxidation of methane (AOM) in sediments of the northeastern South China Sea. Geochimica et Cosmochimica Acta, 246: 138-155.

Dale, A.W. et al., 2019. Kinetics of organic carbon mineralization and methane formation in marine sediments (Aarhus Bay, Denmark). Geochimica et Cosmochimica Acta, 252: 159-178.

Dale, A.W., Van Cappellen, P., Aguilera, D., Regnier, P., 2008. Methane efflux from marine sediments in passive and active margins: Estimations from bioenergetic reaction–transport simulations. Earth and Planetary Science Letters, 265(3-4): 329-344.

Dellwig, O. et al., 2007. Sources and fate of manganese in a tidal basin of the German Wadden Sea. Journal of Sea Research, 57(1): 1-18.

Egger, M., Riedinger, N., Mogollón, J.M., Jørgensen, B.B., 2018. Global diffusive fluxes of methane in marine sediments. Nature Geoscience, 11(6): 421-425.

Fantle, M.S., DePaolo, D.J., 2006. Sr isotopes and pore fluid chemistry in carbonate sediment of the Ontong Java Plateau: Calcite recrystallization rates and evidence for a rapid rise in seawater Mg over the last 10 million years. Geochimica et Cosmochimica Acta, 70(15): 3883-3904.

Fantle, M.S., DePaolo, D.J., 2007. Ca isotopes in carbonate sediment and pore fluid from ODP Site 807A: The Ca2+ (aq)–calcite equilibrium fractionation factor and calcite recrystallization rates in Pleistocene sediments. Geochimica et Cosmochimica Acta, 71(10): 2524-2546.

Froelich, P.N. et al., 1979. Early oxidation of organic matter in pelagic sediments of the eastern equatorial Atlantic: suboxic diagenesis. Geochimica et cosmochimica acta, 43(7): 1075-1090.

Gautschi, W., 1997. Numerical analysis. Springer Science & Business Media.

Holler, T. et al., 2009. Substantial 13C/12C and D/H fractionation during anaerobic oxidation of methane by marine consortia enriched in vitro. Environmental microbiology reports, 1(5): 370-376.

Hu, X., Burdige, D.J., 2007. Enriched stable carbon isotopes in the pore waters of carbonate sediments dominated by seagrasses: Evidence for coupled carbonate dissolution and reprecipitation. Geochimica et Cosmochimica Acta, 71(1): 129-144.

Humphreys, M., Pierrot, D., van Heuven, S., 2020. PyCO2SYS: marine carbonate system calculations in Python. Version 1.3. 0. Zenodo.

This page contains no comments

Jørgensen, B.B., JØrgensen, B.B., Parkes, R.J., 2010. Role of sulfate reduction and methane production by organic carbon degradation in eutrophic fjord sediments (Limfjorden, Denmark). Limnology and Oceanography, 55(3): 1338-1352.

Kaiser, D., Kowalski, N., Böttcher, M.E., Yan, B., Unger, D., 2015. Benthic nutrient fluxes from mangrove sediments of an anthropogenically impacted estuary in Southern China. Journal of Marine Science and Engineering, 3(2): 466-491.

Kastner, M., Elderfield, H., Martin, J., 1991. Fluids in convergent margins: What do we know about their composition, origin, role in diagenesis and importance for oceanic chemical fluxes? Philosophical Transactions of the Royal Society of London. Series A: Physical and Engineering Sciences, 335(1638): 243-259.

Kowalski, N. et al., 2012. A comparative study of manganese dynamics in the water column and sediments of intertidal systems of the North Sea. Estuarine, Coastal and Shelf Science, 100: 3-17.

Kvenvolden, K.A., 1993. Gas hydrates—geological perspective and global change. Reviews of geophysics, 31(2): 173-187.

Lear, C.H., Rosenthal, Y., Slowey, N., 2002. Benthic foraminiferal Mg/Ca-paleothermometry: A revised core-top calibration. Geochimica et Cosmochimica Acta, 66(19): 3375-3387.

Leipe, T., Xia, Z., Gan, H., 2011. RV Sonne Cruise SO219 Report: Holocene Environmental Evolution and Anthropogenic Impact of Beibu Gulf, South China Sea. 35-40.

Lerman, A., Wu, L., Mackenzie, F.T., 2007. CO2 and H2SO4 consumption in weathering and material transport to the ocean, and their role in the global carbon balance. Marine Chemistry, 106: 326-350.

Li, Z., Zhang, Y., Li, Y., Zhao, J., 2010. Palynological records of Holocene monsoon change from the Gulf of Tonkin (Beibuwan), northwestern South China Sea. Quaternary Research, 74(1): 8-14.

Lippmann, F., 1973. Crystal chemistry of sedimentary carbonate minerals, Sedimentary Carbonate Minerals. Springer, pp. 5-96.

Londry, K.L., Des Marais, D.J., 2003. Stable carbon isotope fractionation by sulfate-reducing bacteria. Applied and Environmental Microbiology, 69(5): 2942-2949.

Luff, R., Greinert, J., Wallmann, K., Klaucke, I., Suess, E., 2005. Simulation of long-term feedbacks from authigenic carbonate crust formation at cold vent sites. Chemical Geology, 216(1-2): 157-174.

Luff, R., Haeckel, M., Wallmann, K., 2001. Robust and fast FORTRAN and MATLAB® libraries to calculate pH distributions in marine systems. Computers & Geosciences, 27(2): 157-169.

Luff, R., Wallmann, K., 2003. Fluid flow, methane fluxes, carbonate precipitation and biogeochemical turnover in gas hydrate-bearing sediments at Hydrate Ridge, Cascadia Margin: numerical modeling and mass balances. Geochimica et Cosmochimica Acta, 67(18): 3403-3421.

Luff, R., Wallmann, K., Grandel, S., Schlüter, M., 2000. Numerical modeling of benthic processes in the deep Arabian Sea. Deep Sea Research Part II: Topical Studies in Oceanography, 47(14): 3039-3072.

Mazzini, A., Svensen, H., Hovland, M., Planke, S., 2006. Comparison and implications from strikingly different authigenic carbonates in a Nyegga complex pockmark, G11, Norwegian Sea. Marine Geology, 231(1-4): 89-102.

Meister, P., Liu, B., Ferdelman, T.G., Jørgensen, B.B., Khalili, A., 2013. Control of sulphate and methane distributions in marine sediments by organic matter reactivity. Geochimica et Cosmochimica

This page contains no comments

Acta, 104: 183-193.
Meister, P., Liu, B., Khalili, A., Böttcher, M.E., Jørgensen, B.B., 2019. Factors controlling the carbon isotope composition of dissolved inorganic carbon and methane in marine porewater: An evaluation by reaction-transport modelling. Journal of Marine Systems, 200: 103227.
Middelburg, J.J., Soetaert, K., Hagens, M., 2020. Ocean alkalinity, buffering and biogeochemical processes. Reviews of Geophysics, 58(3): e2019RG000681.
Millero, F.J., 1979. The thermodynamics of the carbonate system in seawater. Geochimica et Cosmochimica Acta, 43(10): 1651-1661.
Millero, F.J., 1995. Thermodynamics of the carbon dioxide system in the oceans. Geochimica et Cosmochimica Acta, 59(4): 661-677.
Mitnick, E.H., Lammers, L.N., Zhang, S., Zaretskiy, Y., DePaolo, D.J., 2018. Authigenic carbonate formation rates in marine sediments and implications for the marine δ13C record. Earth and Planetary Science Letters, 495: 135-145.
Morse, J.W., Mackenzie, F.T., 1990. Geochemistry of sedimentary carbonates. Elsevier.
Morse, J.W., Wang, Q., Tsio, M.Y., 1997. Influences of temperature and Mg: Ca ratio on CaCO3 precipitates from seawater. Geology, 25(1): 85-87.
Mucci, A., 1983. The solubility of calcite and aragonite in seawater at various salinities, temperatures, and one atmosphere total pressure. Am. J. Sci, 283(7): 780-799.
Naehr, T., Rodriguez, N., Bohrmann, G., Paull, C., Botz, R., 2000. 29. Methanederived authigenic carbonates associated with gas hydrate decomposition and fluid venting above the Blake Ridge Diapir, Proceedings of the Ocean Drilling Program, Scientific Results, pp. 285-300.
Ni, S. et al., 2020. Holocene hydrographic variations from the Baltic- North Sea transitional area (IODP site M0059). Paleoceanography and Paleoclimatology, 35(2): e2019PA003722.
Nöthen, K., Kasten, S., 2011. Reconstructing changes in seep activity by means of pore water and solid phase Sr/Ca and Mg/Ca ratios in pockmark sediments of the Northern Congo Fan. Marine Geology, 287(1-4): 1-13.
Peckmann, J. et al., 2001. Methane-derived carbonates and authigenic pyrite from the northwestern Black Sea. Marine geology, 177(1-2): 129-150.
Phrampus, B.J., Hornbach, M.J., 2012. Recent changes to the Gulf Stream causing widespread gas hydrate destabilization. Nature, 490(7421): 527-530.
Regnier, P. et al., 2011. Quantitative analysis of anaerobic oxidation of methane (AOM) in marine sediments: A modeling perspective. Earth-Science Reviews, 106(1-2): 105-130.
Rickaby, R., Schrag, D., Zondervan, I., Riebesell, U., 2002. Growth rate dependence of Sr incorporation during calcification of Emiliania huxleyi. Global biogeochemical cycles, 16(1): 6-1-6-8.
Rodriguez, N., Paull, C., Borowski, W., 2000. 30. Zonation of authigenic carbonates within gas hydrate-bearing sedimentary sections on the Blake Ridge: offshore southeastern north America, Proceedings of the Ocean Drilling Program, Scientific Results, pp. 30.
Rosenthal, Y., Boyle, E.A., Slowey, N., 1997. Temperature control on the incorporation of magnesium, strontium, fluorine, and cadmium into benthic foraminiferal shells from Little Bahama Bank: Prospects for thermocline paleoceanography. Geochimica et Cosmochimica Acta, 61(17): 3633-3643.
Saffer, D.M., Bekins, B.A., 1998. Episodic fluid flow in the Nankai accretionary complex: Timescale, geochemistry, flow rates, and fluid budget. Journal of Geophysical Research: Solid Earth, 103(B12): 30351-30370.

This page contains no comments

Saffer, D.M., McKiernan, A.W., 2009. Evaluation of in situ smectite dehydration as a pore water freshening mechanism in the Nankai Trough, offshore southwest Japan. Geochemistry, Geophysics, Geosystems, 10(2).

Schott, J., Pokrovsky, O.S., Oelkers, E.H., 2009. The link between mineral dissolution/precipitation kinetics and solution chemistry. Reviews in mineralogy and geochemistry, 70(1): 207-258.

Schrag, D.P., Higgins, J.A., Macdonald, F.A., Johnston, D.T., 2013. Authigenic carbonate and the history of the global carbon cycle. science, 339(6119): 540-543.

Sharp, J. et al., 2020. CO2-System-Extd, v3. 0.1, MATLAB (MathWorks).

Soetaert, K., Hofmann, A.F., Middelburg, J.J., Meysman, F.J., Greenwood, J., 2007. Reprint of "The effect of biogeochemical processes on pH". Marine Chemistry, 106(1-2): 380-401.

Sosdian, S.M. et al., 2012. Cenozoic seawater Sr/Ca evolution. Geochemistry, Geophysics, Geosystems, 13(10).

Soulet, G. et al., 2010. Glacial hydrologic conditions in the Black Sea reconstructed using geochemical pore water profiles. Earth and Planetary Science Letters, 296(1-2): 57-66.

Stoll, H.M., Schrag, D.P., 2000. Coccolith Sr/Ca as a new indicator of coccolithophorid calcification and growth rate. Geochemistry, Geophysics, Geosystems, 1(5).

Suess, E. et al., 1999. Gas hydrate destabilization: enhanced dewatering, benthic material turnover and large methane plumes at the Cascadia convergent margin. Earth and Planetary Science Letters, 170(1-2): 1-15.

Sun, X., Turchyn, A.V., 2014. Significant contribution of authigenic carbonate to marine carbon burial. Nature Geoscience, 7(3): 201-204.

Tanabe, S., Hori, K., Saito, Y., Haruyama, S., Kitamura, A., 2003. Song Hong (Red River) delta evolution related to millennium-scale Holocene sea-level changes. Quaternary Science Reviews, 22(21-22): 2345-2361.

Tang, J., Dietzel, M., Böhm, F., Köhler, S.J., Eisenhauer, A., 2008. Sr2+/Ca2+ and 44Ca/40Ca fractionation during inorganic calcite formation: II. Ca isotopes. Geochimica et Cosmochimica Acta, 72(15): 3733-3745.

Teichert, B.M., Gussone, N., Eisenhauer, A., Bohrmann, G., 2005. Clathrites: archives of near-seafloor pore-fluid evolution (δ44/40Ca, δ13C, δ18O) in gas hydrate environments. Geology, 33(3): 213-216.

Trung, N.N., 2012. The gas hydrate potential in the South China Sea. Journal of petroleum science and engineering, 88: 41-47.

Turchyn, A.V., Bradbury, H.J., Walker, K., Sun, X., 2021. Controls on the precipitation of carbonate minerals within marine sediments. Frontiers in Earth Science, 9: 57.

Ussler III, W., Paull, C.K., 2008. Rates of anaerobic oxidation of methane and authigenic carbonate mineralization in methane-rich deep-sea sediments inferred from models and geochemical profiles. Earth and Planetary Science Letters, 266(3-4): 271-287.

Wallmann, K. et al., 2006. Kinetics of organic matter degradation, microbial methane generation, and gas hydrate formation in anoxic marine sediments. Geochimica et Cosmochimica Acta, 70(15): 3905-3927.

Wallmann, K. et al., 2008. Silicate weathering in anoxic marine sediments. Geochimica et Cosmochimica Acta, 72(12): 2895-2918.

Wallmann, K. et al., 2012. The global inventory of methane hydrate in marine sediments: A theoretical approach. Energies, 5(7): 2449-2498.

This page contains no comments

Wang, J., Wu, S., Yao, Y., 2018. Quantifying gas hydrate from microbial methane in the South China Sea. Journal of Asian earth sciences, 168: 48-56.

Whiticar, M.J., Faber, E., Schoell, M., 1986. Biogenic methane formation in marine and freshwater environments: CO2 reduction vs. acetate fermentation—isotope evidence. Geochimica et Cosmochimica Acta, 50(5): 693-709.

Wu, D., Wang, Y., Lin, X., Yang, J., 2008. On the mechanism of the cyclonic circulation in the Gulf of Tonkin in the summer. Journal of Geophysical Research: Oceans, 113(C9).

Wu, Z., Liu, B., Escher, P., Kowalski, N., Böttcher, M., 2018. Carbon diagenesis in different sedimentary environments of the subtropical Beibu Gulf, South China Sea. Journal of Marine Systems, 186: 68-84.

Yang, S. et al., 2015. Preliminary results of China's third gas hydrate drilling expedition: a critical step from discovery to development in the South China Sea. Center for Natural Gas and Oil, 412: 386-7614.

Zeebe, R.E., Wolf-Gladrow, D., 2001. CO2 in seawater: equilibrium, kinetics, isotopes. Gulf Professional Publishing.

Zhang, G. et al., 2015. Geological features, controlling factors and potential prospects of the gas hydrate occurrence in the east part of the Pearl River Mouth Basin, South China Sea. Marine and Petroleum Geology, 67: 356-367.

Zhang, S., DePaolo, D.J., 2020. Equilibrium calcite-fluid Sr/Ca partition coefficient from marine sediment and pore fluids. Geochimica et Cosmochimica Acta, 289: 33-46.

This page contains no comments

Table 1

Sampling locations, water depths, core lengths.

Site/core	Latitude (N)	Longitude (E)	Water depth (m)	Core length (m)
SO-8	18° 41.52′	107° 16.85′	63	8.1
SO-23	19° 21.78′	108° 17.89′	41	7.8
SO-26	18° 28.43′	107° 33.16′	58	6.0
SO-45	19° 55.31′	108° 53.37′	45	5.4
SO-50	20° 25.57′	109° 00.49′	37	5.8

Table 2

Biogeochemical reactions used in the RTM.

Reactions	Reaction stoichiometry	
Organoclastic sulfate reduction, R_{OSR}	$SO_4^{2-} + 2CH_2O \rightarrow HS^- + 2HCO_3^- + H^+$	R1
AOM, R_{AOM}	$CH_4 + SO_4^{2-} \rightarrow HS^- + HCO_3^- + H_2O$	R2
Methanogenesis, R_{ME}[a]	$2CH_2O \rightarrow CH_4 + CO_2$	R3
Authigenic carbonate precipitation, R_{AC}	$Ca^{2+} + 2HCO_3^- \rightarrow CaCO_3 + CO_2 + H_2O$	R4

[a] The net reaction for methanogenesis summarizes the fermentation process of the organic matter and the reduction process of carbon dioxide:

$2CH_2O + 2H_2O \rightarrow 2CO_2 + 4H_2$

$CO_2 + 4H_2 \rightarrow CH_4 + 2H_2O$

These two reactions are considered separately for simulating δ^{13}C-DIC.

Table 3

Rate expression applied in the biogeochemical reactions ($\sum R$ in the Eqs. (7) and (8)).

Variable	Rates
TOC	$-R_{OM}$
SO_4^{2-}	$-0.5 \cdot R_{SR} - R_{AOM}$
CH_4	$0.5 \cdot R_{ME} - R_{AOM}$
DIC	$R_{SR} + R_{AOM} + 0.5 \cdot R_{ME} - R_{AC}$
TA	$R_{SR} + 2 \cdot R_{AOM} - 2 \cdot R_{AC}$
Ca^{2+}	$-R_{AC}$
Mg^{2+}	$-R_{Mg}$
Sr^{2+}	$-R_{Sr}$
δ^{13}C-DIC	${}^{13}R_{SR} + {}^{13}R_{AOM} + {}^{13}R_{Ferm} - {}^{13}R_{ME} - {}^{13}R_{AC}$
δ^{13}C-CH_4	$-{}^{13}R_{AOM} + 0.5 \cdot {}^{13}R_{ME}$
δ^{13}C-AC	${}^{13}R_{AC}$

Page: 40

Number: 1 Subject: Sticky Note Date: 16/07/2022 16:51:25

We are missing the Equilibrium conditions
eg: Carbonic acid dissociation
$H_2CO_3 = HCO_3 + H +$
...

Table 4

List of the definition of symbols and parameters used in the paper.

Parameter	Symbol	Value [a]	Unit	Type [b]	Source [c]
Parameters of physical conditions					
Sediment temperature	T	8	°C	I	v
Bottom water salinity	S	35	-	I	i
Pressure at the SWI	P	4	atm	I	i
Dry sediment density	ρ_S	2.6	g cm^{-3}	I	i
Sedimentation rate	w_f	Var	cm yr^{-1}	III	v
Sediment porosity at the SWI	φ_0	0.7	-	I	v
Sediment porosity at infinite depth	φ_f	0.4	-	I	v
Depth attenuation coefficient of porosity	λ	1/150	m^{-1}	I	v
Simulation length of sediment	L	Var	m	III	v
Diffusion coefficient for SO_4^{2-}	D_{SO}	0.0214	m^2 yr^{-1}	I	iii
Diffusion coefficient for CH_4	D_{CH}	0.0334	m^2 yr^{-1}	I	iii
Diffusion coefficient for DIC	D_{DIC}	0.0232	m^2 yr^{-1}	I	iii
Diffusion coefficient for TA	D_{TA}	0.0212	m^2 yr^{-1}	I	iii
Diffusion coefficient for Ca^{2+}	D_{Ca}	0.0133	m^2 yr^{-1}	I	iii
Diffusion coefficient for Mg^{2+}	D_{Mg}	0.0124	m^2 yr^{-1}	I	iii
Diffusion coefficient for Sr^{2+}	D_{Sr}	0.0129	m^2 yr^{-1}	I	iii
Parameters of biogeochemical reactions					
γ-RCM-parameter	a	Var	yr	III	v
γ-RCM-parameter	v	Var	-	III	v
The content of TOC at the SWI	$G(0)$	Var	wt.%	III	v
Kinetic constant for AOM	k_{AOM}	Var	mM yr^{-1}	III	v
Kinetic constant for Ca^{2+} precipitation	k_{Ca}	Var	mM yr^{-1}	III	v
The equilibrium partition coefficient of Mg^{2+}	K_{Mg}	Var	-	III	v
The equilibrium partition coefficient of Sr^{2+}	K_{Sr}	Var	-	III	v
Depth of the SMTZ	Z_{SMTZ}	Var	m	III	v
Unit conversion factor for organic matter	f_C	Var	-	III	v
Unit conversion factor for carbonate	f_{Ca}	Var	-	III	v
The molecular weight of carbon	M_C	12	g mol^{-1}	I	v
The molecular weight of carbonate	M_{Ca}	100	g mol^{-1}	I	v
Threshold sulfate concentration for ME	C_S^*	1	mM	II	ii
Parameter determining shape of the error function	b	0.001	-	II	ii
The saturation state of calcite	Ω_{cal}	Var	-	III	v
The saturation state of aragonite	Ω_{ara}	Var	-		v
VPDB standard	R_{VPDB}	0.01118	-	II	iv
$\delta^{13}C$ of DIC in sediments	$\delta^{13}C$-DIC	Var	‰	III	v
The fractionation factor for DIC by OSR	α_{SR}	1	-	II	iv
The fractionation factor for DIC by AOM	α_{AOM}	1.02	-	II	iv
The fractionation factor for DIC by ME	α_{ME}	1.04	-	II	iv
The fractionation factor for DIC by AC formation	α_{AC}	1	-	II	iv

[a] Value: Var = the values of these parameters was determined by fitting data from different sites.

Page: 41

Number: 1 Subject: Sticky Note Date: 16/07/2022 16:52:34

I didn't paid attention if you give any justifictionfor it in the descripition of the model, is it the case ?

Number: 2 Subject: Sticky Note Date: 16/07/2022 16:53:22

same than previous comment

Number: 3 Subject: Sticky Note Date: 16/07/2022 16:52:03

I don't think you need a reference for that !
check for other obvious value.

[b] Type: Ⅰ = typical value for marine sediments, Ⅱ = model parameter imposed *a priori*, Ⅲ= model parameter constrained by the date of this study.

[c] Source: (i) Flury et al. (2016), (ii) Chuang et al. (2019), (iii) Boudreau. (1997), (iv) Dale et al. (2019), (v) this study.

Table 5

The best fit parameters at each site.

Variable	SO-8	SO-23	SO-26	SO-45	SO-50
Simulation length of sample, L (m)	12	8	8	5	6
Sedimentation rate, w (cm yr^{-1})	0.03	0.03	0.03	0.04	0.08
TOC content at the SWI (wt.%)	1.0	0.81	1.1	1.1	0.95
γ-RCM-parameter, a (yr)	1324	4315	2831	2419	3410
γ-RCM-parameter, ν_R (-)	0.28	0.21	0.25	0.27	0.29
AOM kinetic constant, k_{AOM} (mM yr^{-1})	0.01	0.03	0.03	-	-
Ca^{2+} precipitation kinetic constant, k_{Ca} (yr^{-1})	0.0007	0.0016	0.0023	0.0002	0.0005
Mg^{2+} equilibrium partition coefficient, k_{Mg} (-)	0.009	0.007	0.008	0.002	0.003
Depth of the SMTZ, Z_{SMTZ} (m)	8.03	5.56	5.32	-	-
Upper boundary of SO_4^{2-} (mM)	30	29.5	29.5	29.5	28.5
Upper boundary of Ca^{2+} (mM)	9.6	10.6	10.6	10	10.8
Upper boundary of Mg^{2+} (mM)	54.1	56.8	57.9	54.8	58.1
Upper boundary of DIC (mM)	1.7	2.1	2.1	2.1	2.1
Upper boundary of TA (mM)	2.2	2.2	2.2	2.2	2.2
Lower boundary of CH_4 (mM)	0→16	0→25	0→20	-	-

Table 6

Depth-integrated rates of OM degradation, OSR, AOM, AC and ME.

Rate or flux	SO-8	SO-23	SO-26	SO-45	SO-50
TR_{OM}, (mol m^{-2} yr^{-1})	0.2922	0.1437	0.2418	0.2870	0.1226
TR_{OSR}, (mol m^{-2} yr^{-1})	0.0514	0.0217	0.0543	0.1435	0.0613
TR_{AOM}, (mol m^{-2} yr^{-1})	0.0394	0.1282	0.1164	-	-
TR_{AC}, (mol m^{-2} yr^{-1})	0.0089	0.0347	0.0365	0.0026	0.0022
TR_{ME}, (mol m^{-2} yr^{-1})	0.0132	0.0066	0.0124	-	-

Page: 42

Number: 1 Subject: Sticky Note Date: 16/07/2022 16:55:37

always good to repeat sepecific acronyms in tables.
cehck in other tables

Table 7

K_{Sr} values determined at the ODP sites and at our study sites.

Site	Temperature (℃)	K_{Sr}	Source
ODP Site 925	17.0	0.023	Zhang et al. (2020)
ODP Site 926	16.4	0.027	Zhang et al. (2020)
ODP Site 927	10.7	0.021	Zhang et al. (2020)
ODP Site 928	12.8	0.023	Zhang et al. (2020)
ODP Site 807	5.4	0.021	Zhang et al. (2020)
SO-8	8	0.025	this study
SO-23	8	0.027	this study
SO-26	8	0.028	this study
SO-45	8	0.021	this study
SO-50	8	0.021	this study

Table 8

SMTZ depth, sulfate and methane fluxes diffusion into SMTZ in Type I sites.

Leg [a]	Site [a]	Water depth (m)	SMTZ (mbsf)	$J_{Methane}$[b] (mM m^{-2} d^{-1})	TR_{AC}[c] (mol m^{-2} yr^{-1})	Description
181	1119	393	14.7	0.0074	0.00135	Continental margin
308	1319	1450	13	0.0096	0.00182	Continental margin
204	1245	870	7.6	0.0208	0.00148	Continental margin
202	1232	4072	23.4	0.0175	0.002	Continental margin
175	1082	1279	20.4	0.0282	0.00243	Upwelling zone
175	1084	1992	5.6	0.0291	0.00186	Upwelling zone
112	688	3827	36.2	0.0066	0.000876	Continental margin
117	725	312	90	0.0111	0.000684	Continental margin
157	951	5437	54	0.0033	0.000262	Deep sea

[a] Mark the cruise and core number of ocean drilling initiatives to which this drilling core belongs.

[b] Fluxes of CH_4 into the SMTZ ($J_{Methane}$) were calculated using their respective porewater concentration gradients above and below the SMTZ (Egger et al., 2018).

[c] The depth-integrated authigenic carbonate formation rate (R_{AC}) were collected from (Mitnick et al., 2018).

This page contains no comments

Table 9

The fraction of authigenic carbonate in the bulk carbonate.

Site	w ($m\ yr^{-1}$)	X_{Carb}[a] (wt.%)	$Flux_{Carb}$ (mM yr^{-1})	$Flux_{AC}$ (mM yr^{-1})	f_{AC}[b] (%)	f_{AC}[c] (%)
SO-8	0.0003	5.9	0.4781	0.0089	1.9	8.9
SO-23	0.0003	7.0	0.5671	0.0347	6.1	3.1
SO-26	0.0003	8.3	0.6724	0.0365	5.4	2.1
SO-45	0.0004	4.4	0.2377	0.0026	1.1	1.1
SO-50	0.0008	3.3	0.3563	0.0022	0.6	1.2

[a] X_{Carb} =kg carbonate/kg sediment averaged over sampling depth (Fig. 2F and Fig. 3F).

[b] Calculate by method from Mitnick et al., 2018.

[c] Results from our model.

Table 10

Global budget of authigenic carbonate formation in different depth regions.

Region (water depth) (m)	Seafloor area[a] (km^2)	SMTZ[a] (mbsf)	J_{CH}[a] (mM m^{-2} d^{-1})	R_{AC} (Tmol yr^{-1})
Inner shelf (0-10)	2.59×10^6	0.5 (±0.7)	0.87 (±0.67)	0.1072
Inner shelf (10-50)	9.18×10^6	2.0 (±2.0)	0.27 (±0.26)	0.1267
Out shelf (50-200)	1.27×10^7	4.0 (±3.1)	0.13 (±0.12)	0.0987
Slope (200-2000)	3.01×10^7	12.8 (±12.1)	0.051 (±0.048)	0.0742
Rise (2000-3500)	6.28×10^7	143.4 (±222.0)	0.0066 (±0.0054)	0.0473
Abyss (>3500)	2.38×10^8	168.9 (±144.5)	0.0047 (±0.0037)	0.0409

[a] the data were collected from Egger et al. (2018)

Page: 44

Number: 1 Subject: Sticky Note Date: 16/07/2022 16:56:17

could we have the amount of carbontes in mol and in kg ?

Figure Captions

Fig. 1. Locations of the sampling sites. Sites SO-8, SO-23, and SO-26 are defined as *Group* I, where bottom SO_4^{2-} was fully consumed. Sites SO-45 and SO-50 were defined as *Group* II, where SO_4^{2-} in the porewater were not completely consumed (Mitnick et al., 2018; Wu et al., 2018).

Fig. 2. Modeled results (curves) and measured data (symbols) at the *Group* I site. A: OM profile. B: SO_4^{2-} and CH_4 profiles. C: DIC, TA, and pH profiles. D: Ca^{2+} profiles. Black, pink, and blue dotted lines denote Ω=1, aragonite saturation, and calcite saturation with below the *x*-axis, respectively. E: Sr^{2+} and Mg^{2+} profiles. F: Solid carbonate and produced solid authigenic carbonate (AC) profiles. G: δ^{13}C-DIC and δ^{13}C-CH_4 profiles. H: δ^{13}C-$CaCO_3$ and δ^{13}C-AC profiles.

Fig. 3. Measured and modeled geochemical profiles of OM, SO_4^{2-}, CH_4, DIC, TA, pH, Ca^{2+}, Sr^{2+}, Mg^{2+}, solid carbonate, produced AC, δ^{13}C-DIC, δ^{13}C-CH_4, δ^{13}C-AC and δ^{13}C-$CaCO_3$ at the *Group* II site. The markers in this figure are the same as in Fig. 2.

Fig. 4. Rate of AOM and authigenic carbonates formation in sites SO-8, SO-23, SO-26, SO-45, and SO-50. The red curves denote the AOM rate with the upper *x*-axis and the blue curves represent authigenic carbonate formation below the *x*-axis, respectively.

Fig. 5. A. Plot of Sr^{2+}/Ca^{2+} versus Mg^{2+}/Ca^{2+} in the porewater. The two black straight lines indicate the trend of Sr^{2+}/Ca^{2+} versus Mg^{2+}/Ca^{2+} in porewater during the formation of aragonite or high Mg-calcite (Bayon et al., 2007; Nöthen and Kasten, 2001). B. Relationship between solid Sr/Ca and Mg/Ca in sediments. The pentagrams and black circle denote the range end-member ratios of detrital fraction (terrigenous clay-rich material, e.g., Al, Si, K, incorporated in the carbonate matrix during authigenic carbonate formation), aragonite, biogenic calcite, and high Mg-calcite, respectively (Bayon et al., 2007). The different symbols in A and B represent the same site. C. High Mg-calcite was observed by electron microscopy within SMTZ at SO-23.

Fig. 6. Sensitivity analysis of high Mg-calcite and aragonite formation in the sediments based on the measured date at site SO-23. A: Depth-profile of Sr^{2+}, Ca^{2+} and Mg^{2+} B: Depth-profiles of high Mg-calcite formation ratio, $f_{cal}(x)$, and the fraction of aragonite can be calculated as: $f_{ara}(x)=1-f_{cal}(x)$. C: Total ratio of high Mg-calcite and aragonite formed in the sediment (B_i at the center of the circle corresponds to B_i in Fig. B). D: Plot of Sr^{2+}/Ca^{2+}versus Mg^{2+}/Ca^{2+} (top inset: magnification of D in *x*-axis 0 to 10 and *y*-axis 0.008-0.013). In A, B, and D, pink color denote that high Mg-calcite was ignored, and the solid, dotted, and dashed lines denote the ratio of high Mg-calcite in the SMTZ of 90%, 70%, and 50%, respectively.

Fig. 7. Impact of non-steady-state for AOM and authigenic carbonate formation based on the measured date at SO-23. A: profiles of SO_4^{2-} (red) and CH_4 (blue). B: profiles of Ca^{2+}. Profiles of AOM rate (red) and authigenic carbonate formation rate (blue). D: profiles of solid-produced authigenic carbonate (AC). E: profiles of δ^{13}C-DIC. F: profiles of δ^{13}C-$CaCO_3$. All the pink solid lines in the figure denote *t*=0 yr that the time point CH_4 starts to seep. The *t*=100 yr, 200 yr, and 400 yr denote the 100, 200, and 400 years after *t*=0 yr with dotted lines, solid lines, and dashed, respectively. The black arrows in the figure indicate the trend of each profile during the non-steady

This page contains no comments

process.

Fig. 8. Depth-integrated AOM rate (TR_{AOM}) and authigenic carbonate formation rate (TR_{AC}) under non-steady-state. A: AOM rate (red) and authigenic carbonate formation rate (blue) versus time (t). The different markers represent different time points shown in the figure and t denotes time after t=0 yr defined in Fig. 7. B: the relationship between AOM rate and authigenic carbonate formation rate (pink: total authigenic carbonate formation (TR_{AC}), blue: AOM-related authigenic carbonate formation (TR_{AOM_AC})) at different time points under non-steady-state, and log-log plot of depth-integrated AOM rate (TR_{AOM}) and authigenic carbonate formation rate (TR_{AC}) (red circles), where TR_{AOM} were replaced by CH_4 flux into the SMTZ (Table 8) under steady-state. Bottom inset in B: magnification of B in x-axis 0.02 to 0.2 and y-axis 0.02-0.05. The red dashed lines in the B denoted 90% confidence bounds of the linear regression meaning the probability of the TR_{AOM} and TR_{AC} being within this range is 90%. The red, blue, and pink arrows in A and B indicate the trend of AOM and authigenic carbonate formation rate during the non-steady process.

Fig. 9. Model sensitivity analysis of CH_4 flux into SMTZ (J_{CH}) based on the measured data at site SO-23. The baseline values are represented by solid curves and the measured data are denoted by red symbols. A: SO_4^{2-} (red) and CH_4 (blue). B: Ca^{2+}. C: AOM rate (red) and authigenic carbonate formation rate (blue). D: δ^{13}C-CH_4 (blue) and δ^{13}C-DIC (red). E: produced solid authigenic carbonate isotope (δ^{13}C-AC, blue) and produced solid authigenic carbonate content (AC, black). F: authigenic carbonate fraction (f_{AC}). G: carbonate isotope (δ^{13}C-$CaCO_3$). All the pink solid lines in the figure denote without CH_4 flux in the bottom sediment, and dotted lines, solid lines and dashed lines denoted different CH_4 flux into the SMTZ shown in the figure.

Fig. 10. The impact of terrestrial- marine transition on authigenic carbonate formation at site SO-8. A: profile of solid $CaCO_3$ and Cl^{-1}. B: SO_4^{2-} and CH_4. C: Ca^{2+} and produced solid authigenic carbonates. D: fraction of produced solid authigenic carbonates and carbonate isotope (δ^{13}C-$CaCO_3$). The red circles and black triangles in B and C denote measured date and corrected data by Cl^{-1} profile, respectively. The pink dotted and solid lines denote the input Cl^{-1} concentrations of 450 mM and 530 mM, respectively. The input SO_4^{2-} and Ca^{2+} concentrations were proportional to Cl^{-1} concentration. The dotted red lines denote the simulation of measured data and solid lines denote the best-fit results of corrected data. The black and red arrows in B indicate the change of SO_4^{2-} profile with increasing Cl^{-1} and methane seep occurred in the bottom sediment.

This page contains no comments

Fig. 1

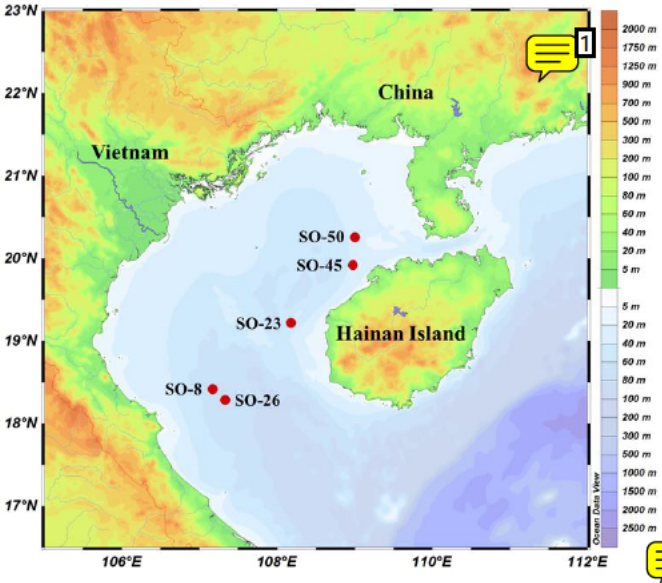

Fig. 1. Locations of the sampling sites. Sites SO-8, SO-23, and SO-26 are defined as *Group* I, where bottom SO_4^{2-} was fully consumed. Sites SO-45 and SO-50 were defined as *Group* II, where SO_4^{2-} in the porewater were not completely consumed (Mitnick et al., 2018; Wu et al., 2018).

Fig. 2

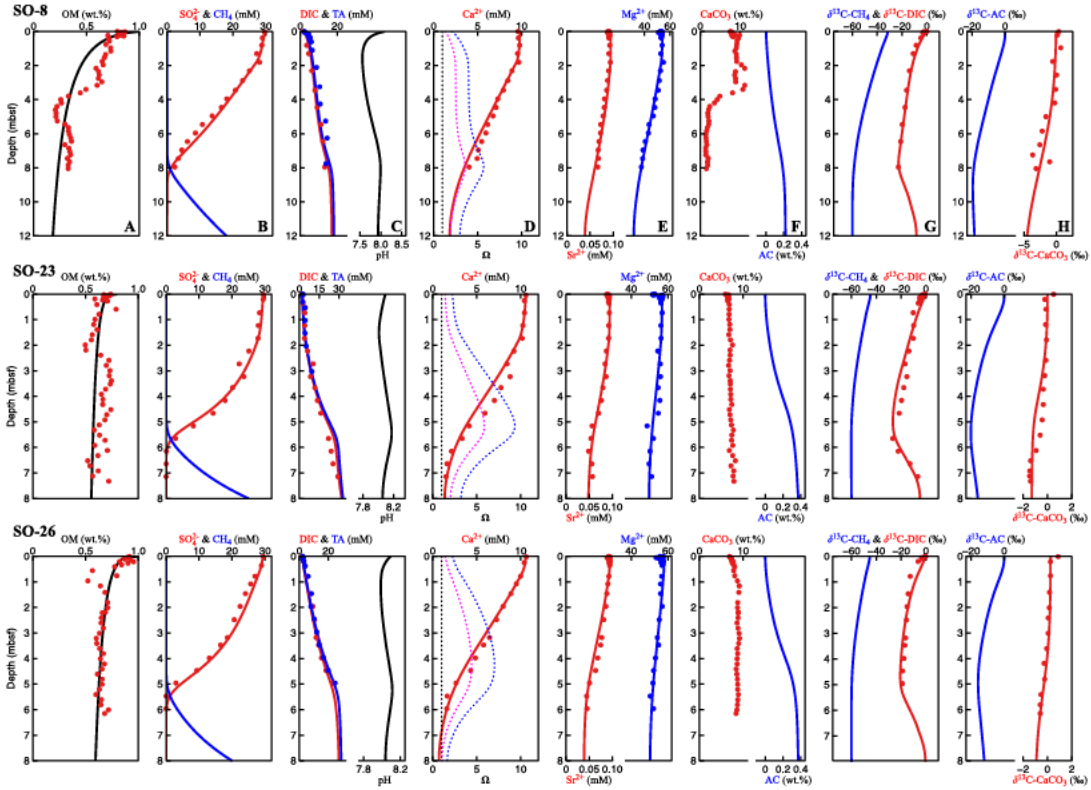

Fig. 2. Modeled results (curves) and measured data (symbols) at the *Group* I site. A: OM profile. B: SO_4^{2-} and CH_4 profiles. C: DIC, TA, and pH profiles. D: Ca^{2+} profiles. Black, pink, and blue dotted lines denote Ω aragonite saturation, and calcite saturation with below the *x*-axis, respectively. E: Sr^{2+} and Mg^{2+} profiles. F: Solid carbonate and produced solid authigenic carbonate (AC) profiles. G: $\delta^{13}C$-DIC and $\delta^{13}C$-CH_4 profiles. H: $\delta^{13}C$-$CaCO_3$ and $\delta^{13}C$-AC profiles.

Page: 47

Number: 1 Subject: Sticky Note Date: 16/07/2022 19:10:04

North; scale.

Number: 2 Subject: Sticky Note Date: 16/07/2022 19:10:41

1 scale (don't repeat meter at each value)

Number: 3 Subject: Sticky Note Date: 16/07/2022 19:11:51

indicate Group 1 and 2 by two differtn colors on your map.

Number: 4 Subject: Sticky Note Date: 16/07/2022 19:07:13

invisible; also, think taht you paper can be printed in black and white.

Number: 5 Subject: Sticky Note Date: 16/07/2022 19:07:37

Omega of which mineral ? Calcite or aragonite ?

Number: 6 Subject: Sticky Note Date: 16/07/2022 19:09:49

Authigenic carbonate (AC) is different from $CaCO_3$? Not clear.

Fig. 3

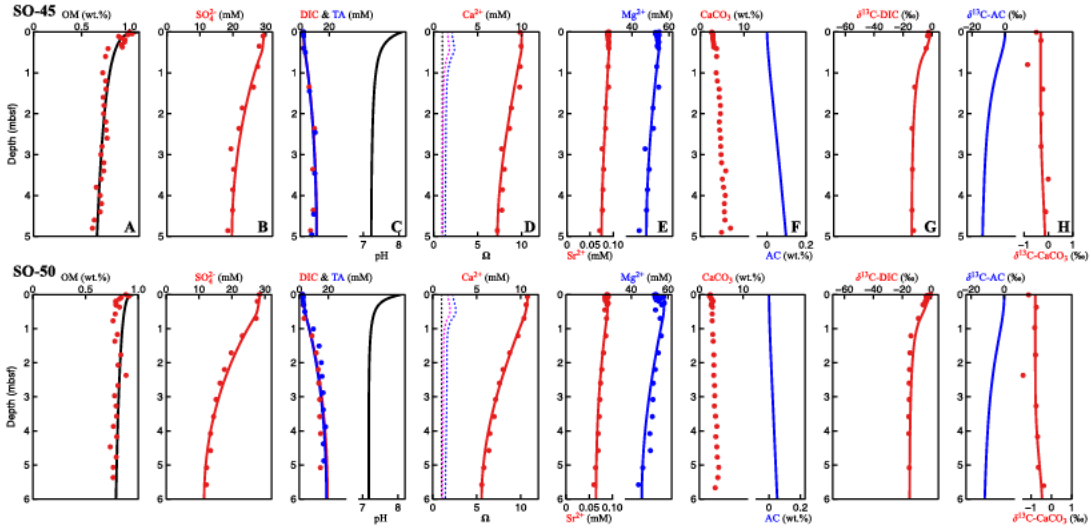

Fig. 3. Measured and modeled geochemical profiles of OM, SO_4^{2-}, CH_4, DIC, TA, pH, Ca^{2+}, Sr^{2+}, Mg^{2+}, solid carbonate, produced AC, δ^{13}C-DIC, δ^{13}C-CH_4, δ^{13}C-AC and δ^{13}C-$CaCO_3$ at the *Group* II site. The markers in this figure are the same as in Fig. 2.

Fig. 4

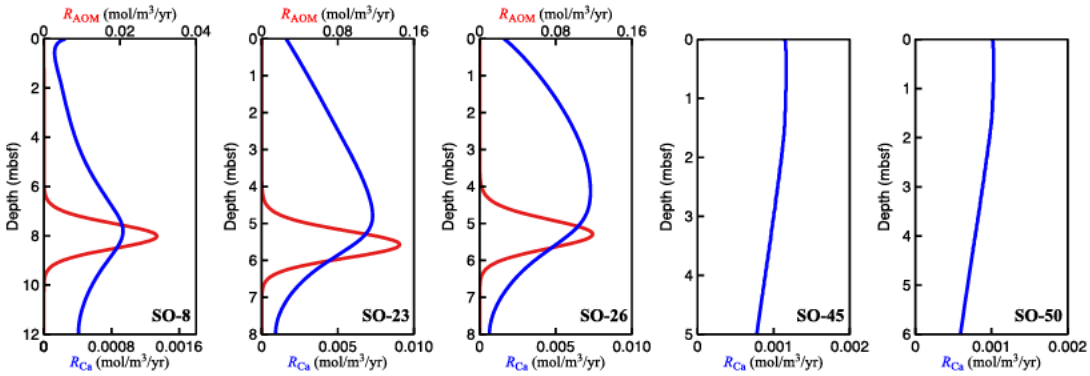

Fig. 4. Rate of AOM and authigenic carbonates formation in sites SO-8, SO-23, SO-26, SO-45, and SO-50. The red curves denote the AOM rate with the upper *x*-axis and the blue curves represent authigenic carbonate formation below the *x*-axis respectively.

Page: 48

Number: 1 | Subject: Sticky Note | Date: 16/07/2022 19:12:07

what do you mean ?

Number: 2 | Subject: Line | Date: 16/07/2022 19:11:50

Fig. 5

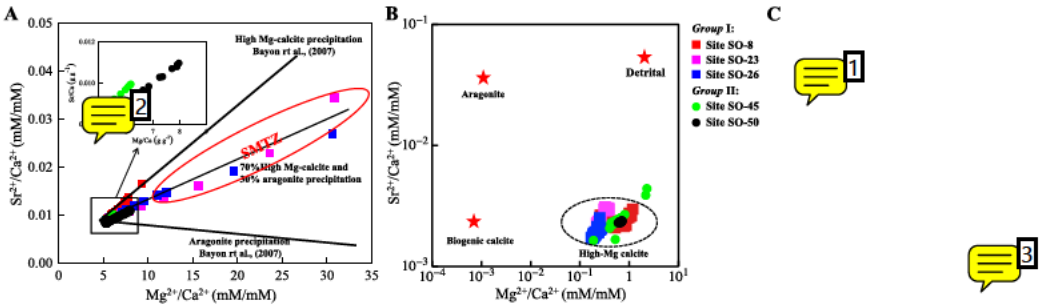

Fig. 5. A. Plot of Sr^{2+}/Ca^{2+} versus Mg^{2+}/Ca^{2+} in the porewater. The two black straight lines indicate the trend of Sr^{2+}/Ca^{2+} versus Mg^{2+}/Ca^{2+} in porewater during the formation of aragonite or high Mg-calcite (Bayon et al., 2007; Nöthen and Kasten, 2001). B. Relationship between solid Sr/Ca and Mg/Ca in sediments. The pentagrams and black circle denote the range end-member ratios of detrital fraction (terrigenous clay-rich material, e.g., Al, Si, K, incorporated in the carbonate matrix during authigenic carbonate formation), aragonite, biogenic calcite, and high Mg-calcite, respectively (Bayon et al., 2007). The different symbols in A and B represent the same site. C. High Mg-calcite was observed by electron microscopy within SMTZ at SO-23.

Fig. 6

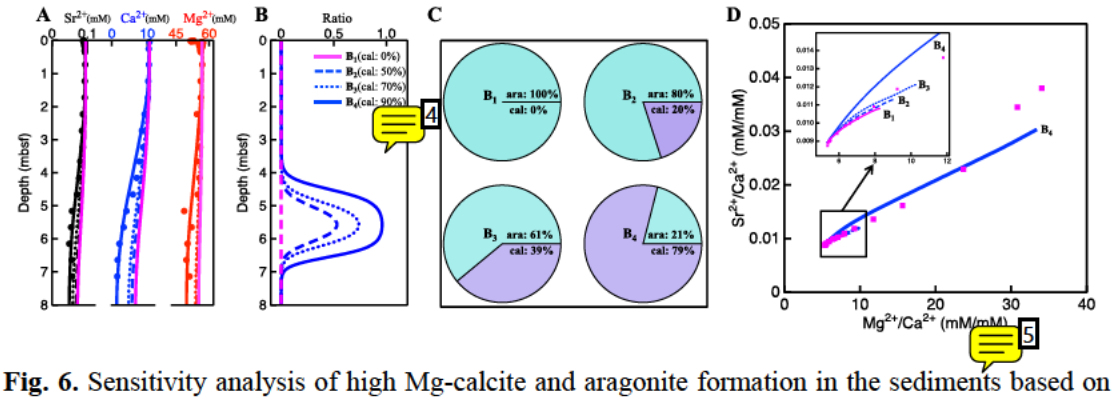

Fig. 6. Sensitivity analysis of high Mg-calcite and aragonite formation in the sediments based on the measured date at site SO-23. A: Depth-profile of Sr^{2+}, Ca^{2+} and Mg^{2+} B: Depth-profiles of high Mg-calcite formation ratio, $f_{cal}(x)$, and the fraction of aragonite can be calculated as: $f_{ara}(x)=1-f_{cal}(x)$. C: Total ratio of high Mg-calcite and aragonite formed in the sediment (B_i at the center of the circle corresponds to B_i in Fig. B). D: Plot of Sr^{2+}/Ca^{2+}versus Mg^{2+}/Ca^{2+} (top inset: magnification of D in *x*-axis 0 to 10 and *y*-axis 0.008-0.013). In A, B, and D, pink color denote that high Mg-calcite was ignored, and the solid, dotted, and dashed lines denote the ratio of high Mg-calcite in the SMTZ of 90%, 70%, and 50%, respectively.

Page: 49

Number: 1 | Subject: Sticky Note | Date: 16/07/2022 19:12:18

informatioin invisible.

Number: 2 | Subject: Sticky Note | Date: 16/07/2022 19:12:38

too small: invisible.

Number: 3 | Subject: Sticky Note | Date: 16/07/2022 19:12:25

idem

Number: 4 | Subject: Sticky Note | Date: 16/07/2022 19:12:51

too small

Number: 5 | Subject: Sticky Note | Date: 16/07/2022 19:14:20

that is, no unit actually.

Fig. 7

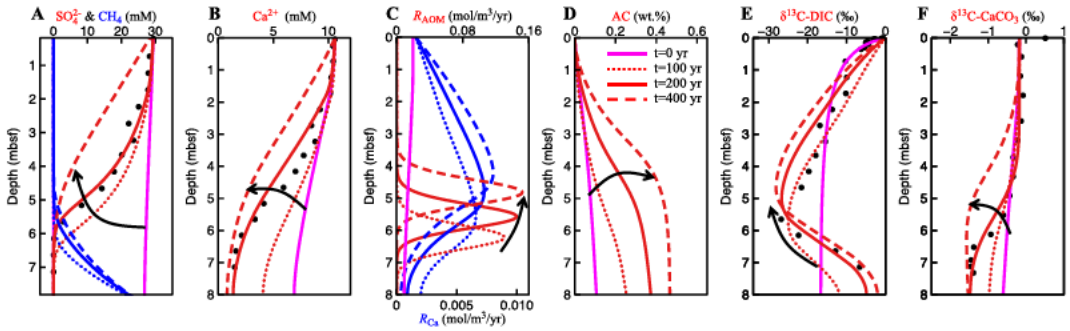

Fig. 7. Impact of non-steady-state for AOM and authigenic carbonate formation based on the measured date at SO-23. A: profiles of SO_4^{2-} (red) and CH_4 (blue). B: profiles of Ca^{2+}. Profiles of AOM rate (red) and authigenic carbonate formation rate (blue). D: profiles of solid-produced authigenic carbonate (AC). E: profiles of δ^{13}C-DIC. F: profiles of δ^{13}C-$CaCO_3$. All the pink solid lines in the figure denote t=0 yr that the time point CH_4 starts to seep. The t=100 yr, 200 yr, and 400 yr denote the 100, 200, and 400 years after t=0 yr with dotted lines, solid lines, and dashed, respectively. The black arrows in the figure indicate the trend of each profile during the non-steady process.

This page contains no comments

Fig.8

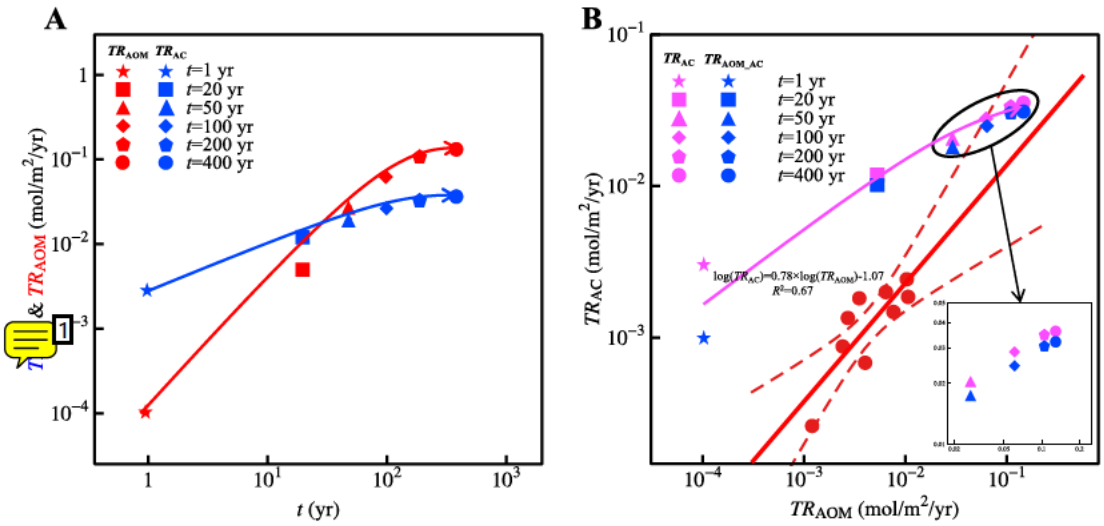

Fig. 8. Depth-integrated AOM rate (TR_{AOM}) and authigenic carbonate formation rate (TR_{AC}) under non-steady-state. A: AOM rate (red) and authigenic carbonate formation rate (blue) versus time (t). The different markers represent different time points shown in the figure and t denotes time after t=0 yr defined in Fig. 7. B: the relationship between AOM rate and authigenic carbonate formation rate (pink: total authigenic carbonate formation (TR_{AC}), blue: AOM-related authigenic carbonate formation (TR_{AOM_AC})) at different time points under non-steady-state, and log-log plot of depth-integrated AOM rate (TR_{AOM}) and authigenic carbonate formation rate (TR_{AC}) (red circles), where TR_{AOM} were replaced by CH_4 flux into the SMTZ (Table 8) under steady-state. Bottom inset in B: magnification of B in x-axis 0.02 to 0.2 and y-axis 0.02-0.05. The red dashed lines in the B denoted 90% confidence bounds of the linear regression ~~meaning the probability~~ of the TR_{AOM} and TR_{AC} ~~being within this range is 90%~~. The red, blue, and pink arrows in A and B indicate the trend of AOM and authigenic carbonate formation rate during the non-steady process.

Page: 51

Number: 1 Subject: Sticky Note Date: 16/07/2022 19:30:04

It could be usefullt to have the amount of carboante in kg; it might be more easy to compare with data than a result in mol

Number: 2 Subject: Line Date: 16/07/2022 19:28:12

Number: 3 Subject: Line Date: 16/07/2022 19:28:05

Fig. 9

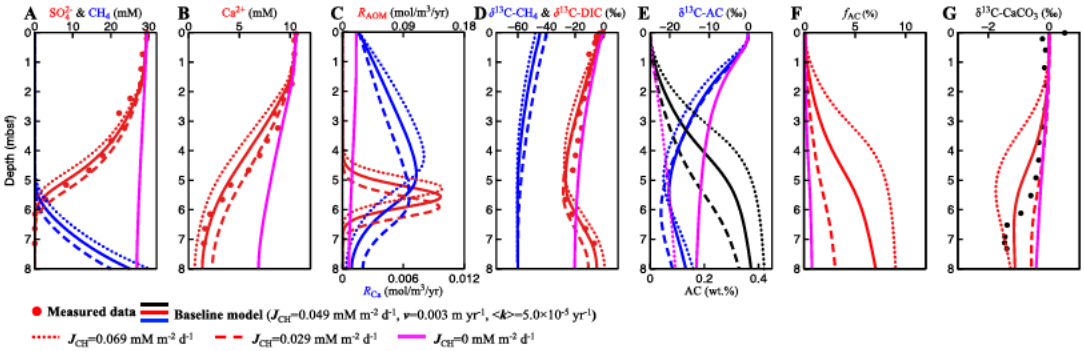

Fig. 9. Model sensitivity analysis of CH_4 flux into SMTZ (J_{CH}) based on the measured data at site SO-23. The baseline values are represented by solid curves and the measured data are denoted by red symbols. A: SO_4^{2-} (red) and CH_4 (blue). B: Ca^{2+}. C: AOM rate (red) and authigenic carbonate formation rate (blue). D: $\delta^{13}C$-CH_4 (blue) and $\delta^{13}C$-DIC (red). E: produced solid authigenic carbonate isotope ($\delta^{13}C$-AC, blue) and produced solid authigenic carbonate content (AC, black). F: authigenic carbonate fraction (f_{AC}). G: carbonate isotope ($\delta^{13}C$-$CaCO_3$). All the pink solid lines in the figure denote without CH_4 flux in the bottom sediment, and dotted lines, solid lines and dashed lines denoted different CH_4 flux into the SMTZ shown in the figure.

Fig. 10

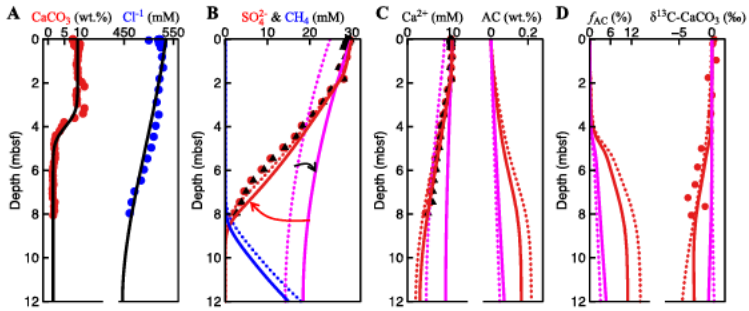

Fig. 10. The impact of terrestrial- marine transition on authigenic carbonate formation at site SO-8. A: profile of solid $CaCO_3$ and Cl^{-1}. B: SO_4^{2-} and CH_4. C: Ca^{2+} and produced solid authigenic carbonates. D: fraction of produced solid authigenic carbonates and carbonate isotope ($\delta^{13}C$-$CaCO_3$). The red circles and black triangles in B and C denote measured date and corrected data by Cl^{-1} profile, respectively. The pink dotted and solid lines denote the input Cl^{-1} concentrations of 450 mM and 530 mM, respectively. The input SO_4^{2-} and Ca^{2+} concentrations were proportional to Cl^{-1} concentration. The dotted red lines denote the simulation of measured data and solid lines denote the best-fit results of corrected data. The black and red arrows in B indicate the change of SO_4^{2-} profile with increasing Cl^{-1} and methane seep occurred in the bottom sediment.

This page contains no comments

This page contains no comments

Supplementary file

This page contains no comments